ACS OMEGA

Open Access

http://pubs.acs.org/journal/acsodf

Review

Challenges and Opportunities of Using Fluorescent Metal Nanocluster-Based Colorimetric Assays in Medicine

Nasim Mohseni, Mohammad Moodi, Amirhosein Kefayat,* Farhad Shokati, and Fatemeh Molaabasi*

Cite This: *ACS Omega* 2024, 9, 3143−3163

Read Online

ACCESS | Metrics & More | Article Recommendations

ABSTRACT: Development of rapid colorimetric methods based on novel optical-active metal nanomaterials has provided methods for the detection of ions, biomarkers, cancers, etc. Fluorescent metal nanoclusters (FMNCs) have gained a lot of attention due to their unique physical, chemical, and optical properties providing numerous applications from rapid and sensitive detection to cellular imaging. However, because of very small color changes, their colorimetric applications for developing rapid tests based on the naked eye or simple UV−vis absorption spectrophotometry are still limited. FMNCs with peroxidase-like activity have significant potential in a wide variety of applications, especially for point-of-care diagnostics. In this review, the effect of using various capping agents and metals for the preparation of nanoclusters in their colorimetric sensing properties is explored, and the synthesis and detection mechanisms and the recent advances in their application for ultrasensitive chemical and biological analysis regarding human health are highlighted. Finally, the challenges that remain as well as the future perspectives are briefly discussed. Overcoming these limitations will allow us to expand the nanocluster's application for colorimetric diagnostic purposes in medical practice.

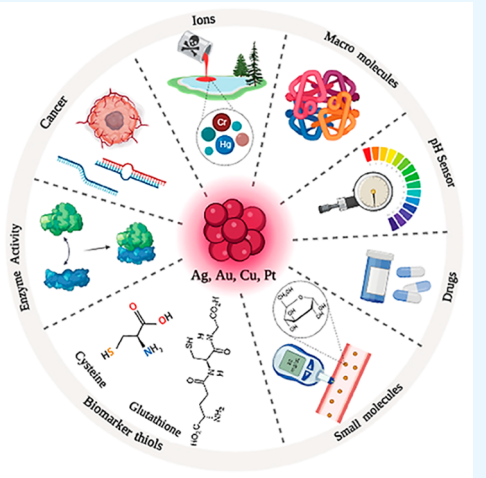

1. INTRODUCTION

1.1. Colorimetric Assays. The development of rapid colorimetric methods is progressing fast, and its importance is deeply sensed, especially in the COVID-epidemic period. Colorimetric assays are easy-to-use, real-time, and affordable methods that can easily identify target molecules by observing color changes. Colorimetric indicators include nanoscale metallic particles, dye molecules, and transducers with selectively interacting capability in the presence of analytes which can lead to a color change.[1−3] The detection technique was used to assess the absorbance of colored compounds at a particular wavelength and visually confirms the existence of analytes.[4] A variety of nanoplatforms are also being used for sensing applications, including carbon dots (CDs),[5] quantum dots (QDs),[6] gold nanoparticles (AuNPs),[7] silver nanoparticles (AgNPs),[8] etc. With a sensitivity below the safe limit concentrations and a regulated error range, it shows considerable promise for semiquantitative and even qualitative analysis.[9] Due to the production of new forms of nanomaterials, the discovery of metal nanoclusters has enhanced research possibilities and gained a lot of attention.[10]

This review highlights the synthesis mechanism of fluorescent metal nanoclusters (FMNCs) and its substantial progress for colorimetric assays. Selected critical applications, including biological and chemical detection, are also discussed and summarized in Table 1. Finally, the current challenges, as well as future perspectives, are briefly discussed. Hopefully, these results can be used to design nanomaterials with the desired functionalities. Additionally, they can be used in various applications to advance their development. To the best of our knowledge, there is no review regarding colorimetric assays for human health based on fluorescent metal nanoclusters.

1.2. Fluorescent Metal Nanoclusters. Noble metal fluorescent nanoclusters, which generally consist of a few to several hundred metal atoms and have diameters between metal atoms and nanoparticles, are quickly expanding due to their unique physical and chemical properties.[11] The diameters of clusters are usually less than 2 nm, which is comparable with the electron Fermi wavelengths of metals. The noble metal nanoclusters exhibit quantum confinement effects together with molecule-like properties (e.g., strong photoluminescence and the lack of a surface plasmon absorption band in comparison to larger metal nanoparticles) because their

Received: September 9, 2023
Revised: November 27, 2023
Accepted: December 14, 2023
Published: January 10, 2024

Table 1. Summary of Fluorescent Metal Nanoclusters Used in Designing Various Colorimetric Sensors Recently

Analyte	Nanocluster	Linear Range	LOD	Real Sample	Ref
Glucose	LNT-PtNCs	5−1000 μM	1.79 μM	Human urine	55
	Keratin-AuNC-Cu^{2+}	1.6−800 μM	0.26 μM	Human serum	68
	GOx&AuNCs@ZIF-8	1.0−25.0 μM	0.8 μM	Human serum	116
	GSH-AuNCs@MCA	100−500 μM	86.9 μM	Human serum	117
	GMP-Au/PtNCs	0.05−0.4 mM	11 μM	Human serum	119
	Yeast extract-PtNCs	0−200 μM	0.28 μM	Human serum	120
	c-myc TBA-Cu/AgNCs	0.1−0.7 mM	9.38 μM	Human serum	73
H_2O_2	c-myc TBA-Cu/AgNCs	0.1−1 mM	7.42 μM	-	73
	GSH-AuNCs	1−10 μM	3.2×10^{-8} μM	Human serum	64
	MSA-CuNCs	1 μM−1 M	0.5 μM	Tap water	104
DA	GLP-Pt_{600}NCs	1−100 μM	0.66 μM	Human serum	56
AA	BGP-PtNCs	1−10 μM	0.191 μM	Milk	57
	BSA-AgNCs	2.0−50.0 μM	0.16 μM	Medicines	107
Pb^{2+}	CS-Au/PtNCs	25 nM−1 mM	16 nM	Milk	59
	GSH-AuNCs	2−250 μM	2 μM	Lake water	65
	MT-CuNCs	707 nM−96 μM	142 nM	Tap water, pond water, and river water	95
Hg^{2+}	MT-CuNCs	97 nM−2.325 μM and 3.10 μM−15.59 μM	43.8 nM	Tap water, pond water, and river water	95
	DNA-Ag/PtNCs	10−200 nM	5.0 nM	Tap water	74
	PAA-AgNCs	0−2 μM	5 nM	Tap water and mineral water	87
	4-chlorothiophenol -CuNCs	1−500 nM	0.3 nM	Tap water, lake water, and wastewater	92
	PRT-AuNCs	4.0 nM−1.0 μM	1.16 nM	Pond water, river water, and tap water	91
	His-AuNCs	0.05−0.8 μM	8 nM	Human serum	70
	GSH-Ag/CuNCs	0.1−700 nM	0.05 nM	Human serum, human urine, seawater, and mineral water	94
	BSA-AuNCs	0.2−60 μM	30 nM	River water	90
Cys	BSA-AuNCs	0.2−60 μM	80 nM	-	90
	GSH-AgNCs	-	-	-	139
	GSH-Au/PtNCs	0.5−30 μM	0.154 μM	Human serum and urine	140
TBHQ	BSA-AuNCs	-	-	Edible and coconut oil samples	67
DNP	L-Histidine-AA-CuNCs	0.01−0.15 mM	3.96 μM	Tap water and river water	69
S. aureus	DNA-Au/PtNCs	108−102 CFU/mL	80 CFU/mL	Human serum, milk, and orange juice	72
E. coli	Aptamer@papain@AuNCs	102−106 cfu mL^{-1}	5.6×10^2, 5×10^2, and 4.9×10^2 cfu mL^{-1}	UHT-sterilized milk, pasteurized milk, and raw milk	76
S. typhimurium	Aptamers@BSA-AuNCs	101−106 cfu mL^{-1}	1 cfu mL^{-1}	Eggshell and egg white	77
Fe^{2+}	PMAA-AgNCs	5−100 μM	76 nM	Ferrous sulfate in deionized water	97
Cr^{6+}	PEI-AgNCs	5−100 μM	1.1 μM	Tap water and lake water	96
Cl^-	PEI-AgNCs	50−400 μM	20 μM	Tap water and mineral water	86
Br^-	PEI-AgNCs	10−300 μM	5 μM	-	86
I^-	PEI-AgNCs	10−200 μM	5 μM	-	86
	His-AuNCs	0.02−1 μM	3.3 nM	Human serum	70
Nitrite	His@AuNCs/RGO	10−500 μM	2 μM	Sausage	98
Sulfide	TA-CuNCs/Cu^{2+}	6.0−130.0 μM	2.0 μM	Rainwater, tap water, wastewater, and Koohrang spring	99
	GSH-CuNCs	0−50 μM	0.5 μM	Tap water and lake water	100
HQ	3DGF-PtNCs	0.05−50 μM	10 nM	-	108
ALP	BSA-AuNCs	1.0−6.0 mU mL^{-1}	0.26 mU mL^{-1}	Human serum	130
GSH	GSH-AuNCs	2−25 μM	420 nM	Human cell lines (THP-1 and HBE) and cancer cell lines (MCF-7 and MDA-MB-231)	143
	Cys-CuNCs	1−150 μM	0.89 μM	GSH tablets in water	144
	Cytidine-AuNCs	0−0.4 mM	0.01 mM	-	145
GSSG	Cytidine-AuNCs	0−2.5 mM	0.03 mM	-	145
GR	Cytidine-AuNCs	0−0.2 U/mL	0.003 U/mL	-	145
Doxycycline	D-His-AuNCs	5.0−12.5 μM	1.0 μM	Rat serum	146
TCs	Aptamer-AuNCs	1−16 μM	46 nM	Milk	147
MA	GSH-AuNCs	0.115−2.3 nM	1 pM	Human blood	148
Bilirubin	BSA-CuNCs	0−300 pM	-	Human urine	102
p-nitrophenol	PEI-AgNCs	5−140 μM	1.28 μM	Tap water, river water, and soils	103
Xanthine	BSA-CuNCs	5.0×10^{-7}−1.0×10^{-4} mol L^{-1}	3.8×10^{-7} mol L^{-1}	Human serum	105
PPi	Keratin-AuNCs-Cu^{2+}	0.51−30,000 nM	0.49 nM	Human urine	106

https://doi.org/10.1021/acsomega.3c06884
ACS Omega 2024, 9, 3143−3163

Table 1. continued

Analyte	Nanocluster	Linear Range	LOD	Real Sample	Ref
Heparinase	BSA-AuNCs	0.1−3 $\mu g \cdot mL^{-1}$	0.06 $\mu g \cdot mL^{-1}$	Fetal bovine serum	121
Thrombin	DNA-Ag/PtNCs	1 nM−50 nM	2.6 nM	Human serum	123
α-amylase	Starch-Cu/AuNCs	0.1−10 U/mL	0.04 U/mL	Human serum	124
Trypsin	BSA-AuNCs	0.9 μg/mL−1.0 mg/mL	0.6 g/mL	Human urine	10
ss-DNA	Au/PtNCs	50 pM−100 nM	4.1 pM	Milk samples	158
miRNA-21	DNA-Ag/PtNCs	1.0−700pM	0.6 pM	Human blood plasma	156
	DNA-CuNCs	1.0 pM−10.0 nM	0.6 pM	Human blood plasma	157
SKBR3 cells	AuNC-loaded liposomes	5−1000 cells	5 cells	Human serum	164
	MSN-AuNCs	10−1000 cells	10 cells	-	165
MCF-7 cells	GO-AuNCs	5−1000 cells	5 cells	-	12
Citrate	Cys-AuNCs	0.5−1000 μM	0.1 μM	Human urine	169

Scheme 1. Schematic Illustration of Different Colorimetric Detection Mechanisms Based on Fluorescent Metal Nanoclusters

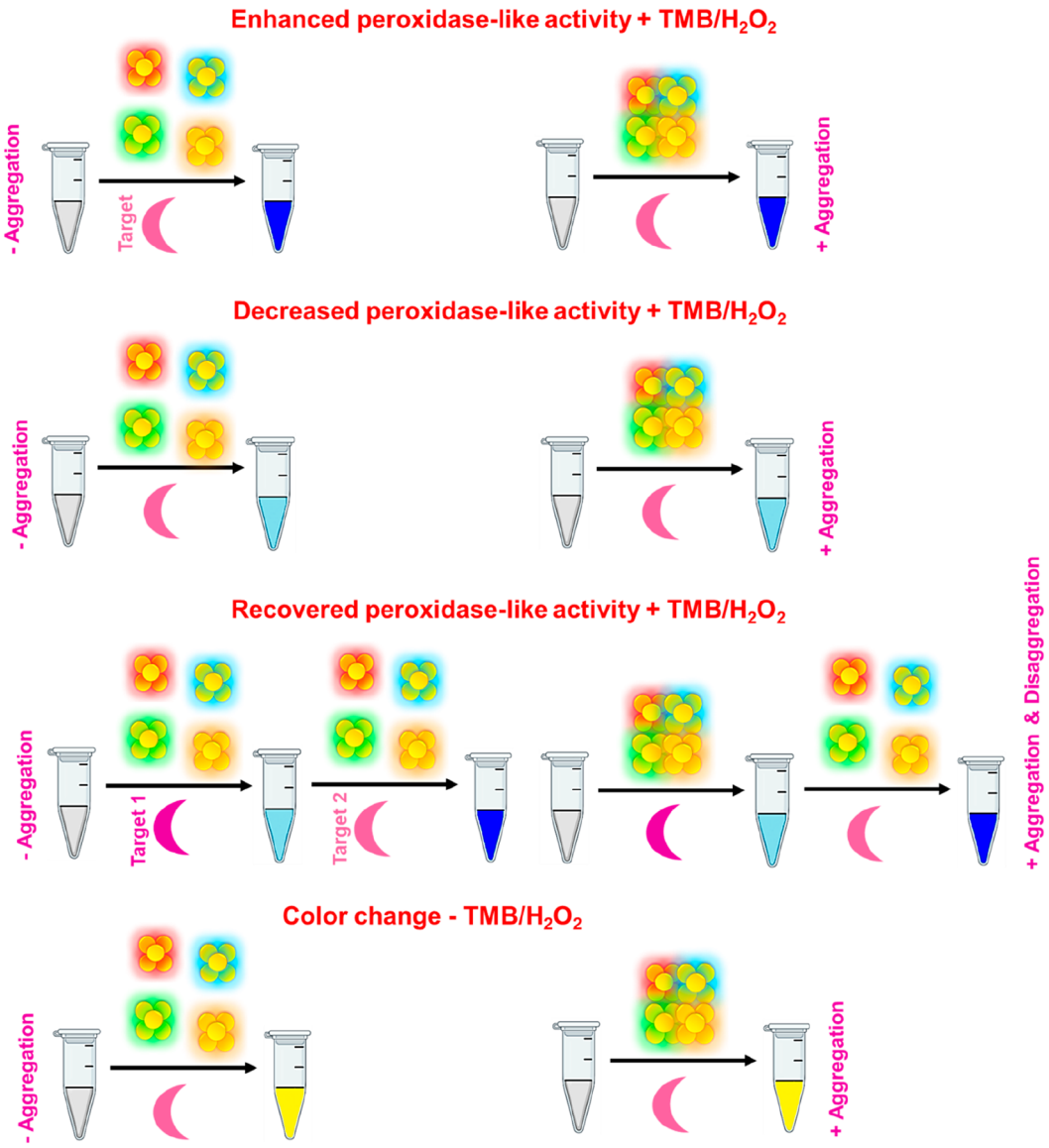

continuous band structure is broken up into discrete energy levels.[2] Moreover, they generally have a ligand shell and a metal core (i.e., Au, Ag, Pt, Cu).[12] Numerous investigations have demonstrated that the fluorescence of metal NCs is sensitive to changes in the microenvironment caused by changes in the electron-transferring mechanism between the metal core and the protected ligand.[13] Several nanoplatforms based on fluorescence metal nanoclusters (FMNCs) have been developed for colorimetric assays because of their high water solubility, good biocompatibility, and rich surface chemistry for

https://doi.org/10.1021/acsomega.3c06884
ACS Omega 2024, 9, 3143−3163

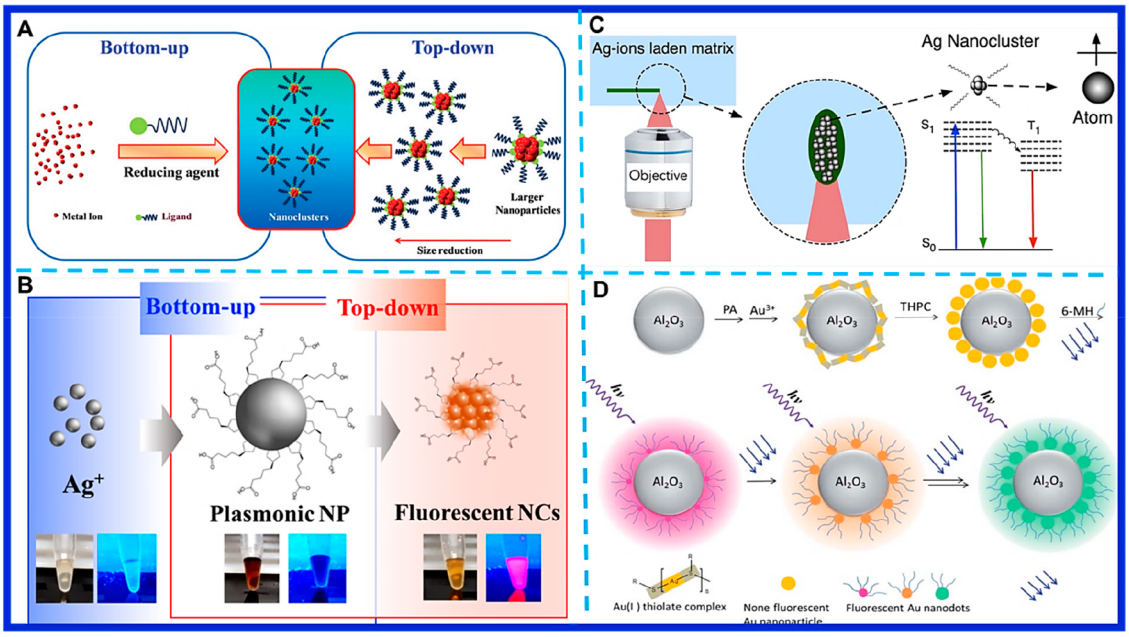

Figure 1. (A) Illustration of FMNC formation by top-down and bottom-up approaches;[16] adapted with permission from ref 16. Copyright 2019 Royal Society of Chemistry. (B) The multistage synthesis of AgNCs using dihydrolipoic acid as a capping agent ($Ag_{29}(DHLA)_{12}$NCs) based on the combination of the bottom-up and top-down synthesis methods;[17] adapted with permission from ref 17. Copyright 2020 American Chemical Society. (C) AgNCs formation by direct laser writing (DLW);[29] adapted with permission from ref 29. Copyright 2020 American Chemical Society. (D) The synthesis of Al_2O_3NP@AuNCs by a top-down approach;[19] adapted with permission from ref 19. Copyright 2019 Royal Society of Chemistry.

conjugation.[14] Due to beneficial characterization, further development of FMNC-based colorimetric assay strategies has gained sufficient popularity and is strongly encouraged. To overcome the limitations of solution-based FMNC biosensors, several nanomaterials, including carbon nanotubes, silica, etc., have been applied as a template for holding FMNCs.[15]

2. DETECTION MECHANISM

The mechanism of most studied NC-based platforms in colorimetric assays is based on the peroxidase-like activity of NCs. In this regard, it can be referred to common reagents, including methylene blue (MB), 3,3′,5,5′-tetramethylbenzidine (TMB), *o*-phenylenediamine (OPD), and 2,2′-azino-bis(3-ethylbenzothiazoline-6-sulfonic acid) (ABTS), which could be catalyzed by NCs. The generated colorimetric signals could be followed and detected by a UV−vis spectrophotometer or via the naked eye. Most of these nanoclusters catalyze the decomposition of H_2O_2 into •OH radicals, resulting in the oxidation of TMB (oxTMB) and thus indicating their peroxidase-like properties. The catalytic reaction on the substrate TMB followed the Michaelis−Menten equation. Moreover, the aggregation or disaggregation of metal nanoclusters in the absence or the presence of TMB/H_2O_2 upon the addition of a target can affect its peroxidase-like activity and so trigger color changes. Also, sometimes a color change happens as a result of a new complex formation or only an electrostatic interaction between the target and FMNCs without any NC aggregation or disaggregation. All of the different proposed detection mechanisms based on FMNCs have been shown in Scheme 1.

3. SYNTHESIS MECHANISM

Fluorescent metal nanoclusters are usually synthesized using top-down and bottom-up methods (Figure 1A, B).[16,17] In the top-down approach, at first metal nanoparticles are formed, and then they are etched by high temperature or by chemical techniques such as direct core reduction and/or the interface etching of large AuNPs by excess thiol ligands in an alkaline solution. 11-Mercaptoundecanoic acid (11-MUA) has been known as an etching agent to stabilize AuNCs by THPC as a reducing and capping agent via a high pH (>12.0).[18] In other work, the efficacy of AuNC synthesis was improved by applying: (i) Al_2O_3NPs modified by penicillamine (PA) in the presence of THPC to further reduce Au^{3+} ions to Au^{+} ions for small AuNP formation and (ii) after further etching as-formed AuNPs by 6-mercaptohexanol under blue LED irradiation (Figure 1D).[19] The highly red emissive AuNCs have also been obtained by etching didodecyldimethylammonium bromide-stabilized AuNPs with dihydrolipoic acid[20] as well as by etching GSH-capped $Au_{25}SG_{18}$ with octanethiol.[21] Ligand-induced etching is another process to prepare polymer-capped NCs. In this case, it can be referred to as replacing the capping agent dodecylamine with polyethylenimine resulting in AuNP etching and thus Au8NC formation with a QY of 10−20%.[22] In another interesting way, the nonfluorescent AuNCs can be converted to highly fluorescent AuNCs (QY ∼ 5.4%) by using the etching agent GSH.[23]

The bottom-up approach induces atom-by-atom construction resulting in ultrasmall NPs with homogeneous chemical compositions and fewer defects (Figure 1A).[16] In this approach, metal ions are reduced to zerovalent metal atoms using various reduction methods such as microwave reduction,[24] photoreduction,[25] chemical reduction,[26] sonochemical reduction,[27] and electrochemical reduction.[28] There are two

https://doi.org/10.1021/acsomega.3c06884
ACS Omega 2024, 9, 3143−3163

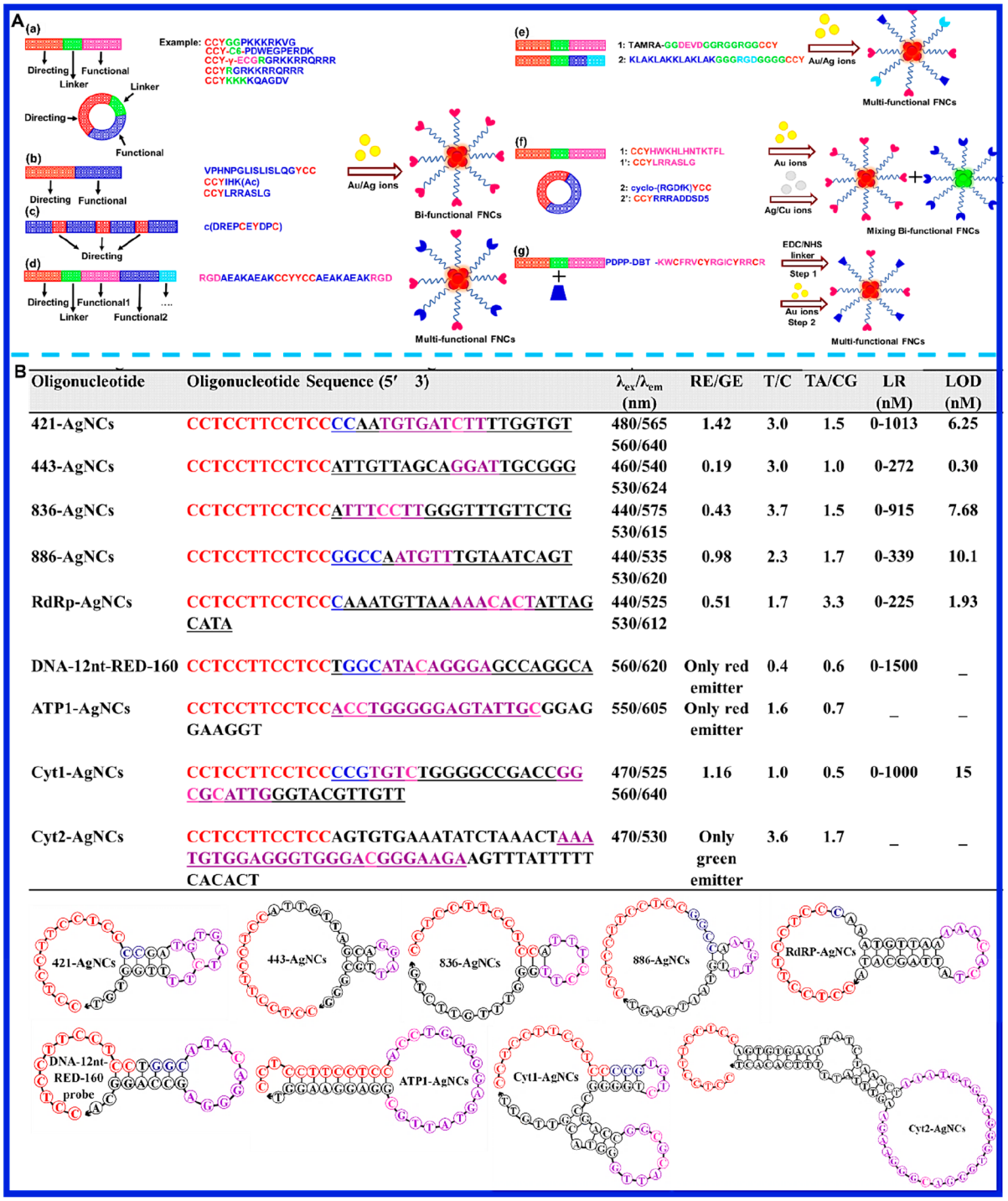

Oligonucleotide	Oligonucleotide Sequence (5′ 3)	$\lambda_{ex}/\lambda_{em}$ (nm)	RE/GE	T/C	TA/CG	LR (nM)	LOD (nM)
421-AgNCs	CCTCCTTCCTCCCCAATGTGATCTTTTGGTGT	480/565 560/640	1.42	3.0	1.5	0-1013	6.25
443-AgNCs	CCTCCTTCCTCCATTGTTAGCAGGATTGCGGG	460/540 530/624	0.19	3.0	1.0	0-272	0.30
836-AgNCs	CCTCCTTCCTCCATTTCCTTGGGTTTGTTCTG	440/575 530/615	0.43	3.7	1.5	0-915	7.68
886-AgNCs	CCTCCTTCCTCCGGCCAATGTTTGTAATCAGT	440/535 530/620	0.98	2.3	1.7	0-339	10.1
RdRp-AgNCs	CCTCCTTCCTCCCAAATGTTAAAAACACTATTAG CATA	440/525 530/612	0.51	1.7	3.3	0-225	1.93
DNA-12nt-RED-160	CCTCCTTCCTCCTGGCATACAGGGAGCCAGGCA	560/620	Only red emitter	0.4	0.6	0-1500	_
ATP1-AgNCs	CCTCCTTCCTCCACCTGGGGGAGTATTGCGGAG GAAGGT	550/605	Only red emitter	1.6	0.7	_	_
Cyt1-AgNCs	CCTCCTTCCTCCCCGTGTCTGGGGCCGACCGG CGCATTGGGTACGTTGTT	470/525 560/640	1.16	1.0	0.5	0-1000	15
Cyt2-AgNCs	CCTCCTTCCTCCAGTGTGAAATATCTAAACTAAA TGTGGAGGGTGGGACGGGAAGAAGTTTATTTTT CACACT	470/530	Only green emitter	3.6	1.7	_	_

Figure 2. (A) Different designs of peptide sequences as capping/reducing agents for the synthesis of bi/multifunctional FMNCs. (a) Designed peptide consists of directing, linker, and functional sequence parts that are used for the synthesis of FMNCs, the connection between directing and functional parts, and targeting function, respectively. (b) Designed peptide without the linker part. (c) Incorporation of directing sequences between the functional sequences. (d) Construction of multifunctional FMNCs by simultaneously applying more than one fictional part. (e) Synthesis of multifunctional FMNCs by using two designed peptides, simultaneously. (f) Preparation of multifunctional FMNC probes via mixing the designed peptide-stabilized NCs, each of which is separately synthesized. (g) Development of an all-in-one theranostic FMNC probe by the covalent attachment between a photothermal conversion agent and the designed targeting peptide using the EDC/NHS linker and also the NIR-light-assisted method;[41] reprinted from ref 41. Copyright 2022 with permission from Elsevier. (B) Different DNA-AgNCs consist of targeting sequences for the N (421-, 443-, 836-, 886-AgNCs) and RdRp genes of SARS-CoV-2, miRNA, ATP, and cytochrome *c* targets with the same cytosine-rich sequences. The predicted structures of designed AgNC probes are also shown in the figure below. Four colors have been used to show different parts of probe sequences: cytosine-rich with red sequences used as a cluster-stabilizing template, cytosine (C) and guanine (G) with blue sequences as the initial residues of the targeting part attached to the cytosine-rich sequence, the loop structure with purple sequences containing pink cytosine, and complementary sequences to the target with black sequences. The targeting sequences are underlined;[42] adapted with permission from ref 42. Copyright 2022 American Chemical Society.

https://doi.org/10.1021/acsomega.3c06884
ACS Omega 2024, 9, 3143−3163

accepted states in the chemical reduction process to form FMNCs: in one a capping agent can act as both a stabilizing and a reducing agent, while in the other, chemical reducing agents such as tetrakis(hydroxymethyl) phosphonium chloride (THPC), sodium borohydride ($NaBH_4$), or sodium hypophosphite ($NaPO_2H_2{\cdot}H_2O$) are used in the presence of the capping agent. Sonochemical reduction is a useful method to produce NCs under ultrasonic irradiation, while in the photoreduction approach, UV and visible lights result in a controlled reduction without any impurity induction and/or using hazardous substances (e.g., $NaBH_4$). For example, blue-emitting AuNCs could be synthesized by tridentate thioether-terminated polymers, i.e., poly(methyl methacrylate), poly(*tert*-butyl methacrylate), and poly(*n*-butyl methacrylate), through photoreduction with QYs of 20.1%, 14.3%, and 3.8%, respectively. Moreover, microwave-assisted reduction is a simple, fast method with high reproducibility, and the electrochemical reduction method produces NCs with well-defined sizes as well. Recently, direct laser writing (DLW) has been developed as a bottom-up approach for synthesizing and patterning NCs in which photostable and high-quantum-yield FMNCs could be formed with precise spatial control leading to the advantage of the creation of easy-to-use solid-state devices for a broad range of applications (Figure 1C).[29]

Key parameters to control the structure, oxidation state, size, and surface properties that affect the optical properties of FMNCs include the species of metal ions and capping agents/templates, the concentration of reducing agents, the mole ratio of metal ions to templates as well as the molar ratio of two metals in bimetallic NCs (Ag^+/Au^{3+}), the reaction time, temperature, and pH of the solution. For example, red-emitting Ag_{28}NCs at pH 12 and blue-emitting Ag_{5-7}NCs were prepared using the same peptide at pH 9. Also, the orange-emitting AuNCs, comprising $Au_{29}SG_{27}$, $Au_{30}SG_{28}$, $Au_{36}SG_{32}$, $Au_{39}SG_{35}$, and $Au_{43}SG_{37}$, were achieved with a Au/peptide mole ratio of ∼2/3 at 70 °C for 24 h. Moreover, both Ag_5NCs and Ag_{15}NCs were synthesized on cytosine-rich ATP1 oligonucleotide at room temperature.[30] Blue-emitting Pt_6NCs and red-emitting Pt_{16}NCs were simultaneously synthesized by human Hb protein at 37 °C and pH 12 with a [Pt]/[Hb] ratio of 1.13.[31] Au_5, Au_{13}, and Au_{25} with blue, green, and red colors could also be synthesized by pepsin at pH values of 9.0, 10.0, and 12.0, respectively.[32] The reaction temperature controls the protein conformation and reaction rate and thus the size of FMNCs. For example, the preparation time of Hb-AgNCs was shortened from 21 days to 10 days and for BSA-AuNCs from 12 h to 20 min when the reactions were conducted at ∼70 °C instead of 37 °C.[33] Different chain lengths of alkanethiols as etching ligands also cause different emission wavelengths from 501 to 613 nm.[34,35]

Except for the above-mentioned factors, in the case of proteins, another important parameter is the flexibility of protein structure so that sometimes the redistribution of metal ions between protein molecules changes the conformation/structure (e.g., $\alpha-\beta$ transition in Hb@AuNCs), leading to the effective formation of NCs which can be confirmed by the UV spectra and circular dichroism (CD).[36,37] In this regard, the biological activity of some proteins such as HRP-AuNCs,[38] Hb-AuNCs,[39] and insulin-AuNCs[40] is maintained even after NC formation. Moreover, the amino acid composition and especially the number ratios of amine/thiol and tyrosine/tryptophan are important in the synthesis conditions of stable luminescent NCs. Notably, Tyr residues with pK_a of ∼10 in proteins and peptides play an important role at basic pH. For example, the phenolic groups of Tyr residues in BSA can reduce Au^{1+} ions into AuNCs after the coordination of Au^{3+} ions with the histidine and cysteine residues and conversion to Au^{1+}. This process can happen in many other proteins such as transferrin family proteins, lysozymes, DNase I, horseradish peroxidase (HRP), hemoglobin (Hb), and ribonuclease A (RNase A), by which AuNCs with 20−25 Au atoms per protein template are usually stabilized.[34]

Regarding peptide ligands as capping agents, the length and amino acid composition are important parameters to tailor the size, lifetime, quantum yield, and thus the emission color of NCs (Figure 2A). The Cys-Cys-Tyr (CCY) fragment is commonly used as both a reducing and stabilizing template for peptide-protected NC formation (Figure 2A). In brief, at first the interaction between metal ions (e.g., Ag, Au, Cu) and thiols of CC results in −SR−[M−SR−]2 intermediates. After that, the negative phenolic group of Y reduces the metal ions to atoms by adjusting pH > 10 with NaOH. Finally, the produced metal atoms aggregate and convert to the metal NCs capped by the thiol groups of peptides. In the absence of Tyr, a strong reducing agent (e.g., $NaBH_4$) is needed for metal ion reduction. To synthesize more stable NCs with enhanced quantum yield, an auxiliary ligand (e.g., mercaptopropionic acid (MPA)) is usually added to the peptide reaction solution. Moreover, to construct bi-/multifunctional peptide-protected NCs for both targeting and sensing, especially in cancer theragnostics, the combination of different functional fragments is proposed (Figure 2A). In this way, the developed peptide usually consists of three parts: directing sequence for NC formation, linker sequence for connecting the directing sequence to recognition parts, and functional or recognition sequence for targeting. The presence of the linker sequence is not essential for designing peptides (Figure 2A).[41]

For DNA ligands, the cytosine presence together with base composition and length of the DNA strand are effective factors in NC formation (Figure 2B). Moreover, regarding two NC species formation by a single DNA strand, key points could be also considered, including cytosine located at the 3′ ends of the NC-stabilizing sequence, the use of a thymine-rich targeting template, the creation of distance between stem-loop structure, and the cluster-stabilizing sequence, with regard to the stem length as well as cytosine number in the loop structure (Figure 2B).[42]

The important functional groups in capping agents/ligands for the effective coordination with metal ions to form NCs are hydroxyl, amine, and thiol which may allow the creation of the M(0)NCs@M(I/II)-ligand core−shell structure (Figure 3A,B). The core−shell structure has been successfully demonstrated for proteins (e.g., BSA-AuNCs, Hb-AgNCs, and Hb-PtNCs),[31,33] peptides (e.g., GSH-AuNCs and GSH-AgNCs), and DNA (e.g., ATP1-AgNCs, Cyt1-AgNCs, and Ngene-AgNCs).[42,43] This has a pivotal role in inducing interesting synthesis mechanisms/approaches, aggregation-induced emission (AIE), and oxidation phenomena (Figure 3A). In the oxidation process, an oxygen etching effect and/or NC core oxidation occurs using O_2 as an oxidant which can promote the charge transfer from the electron-donating surface functional groups present at the ligand layer to the metal core (LMCT/LMMCT) via nitrogen, oxygen, and sulfur atoms. In the AIE mechanism, the NC aggregation happens which is controlled by the intra- and intercomplex metallophilic M(I/II)···M(I/II) interactions (M: Au, Pt, Ag, Cu), resulting in a

https://doi.org/10.1021/acsomega.3c06884
ACS Omega 2024, 9, 3143−3163

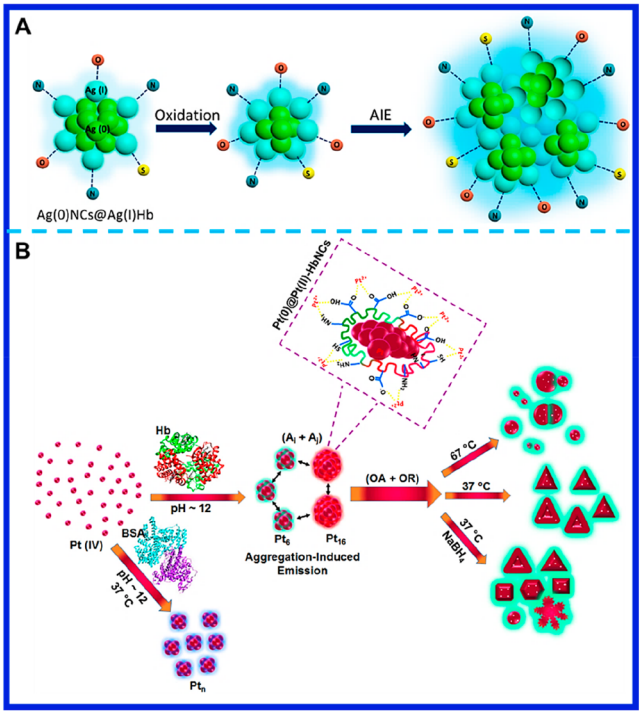

Figure 3. (A) Illustration of AgNC formation using human hemoglobin (Hb) as a stabilizing/reducing agent based on the combination of the NC core oxidation and aggregation-induced emission (AIE) approaches;[33] adapted with permission from ref 33. Copyright 2018 American Chemical Society. (B) The synthesis of various porous hollow fluorescent Hb-templated Pt nanostructures through a combination of AIE, oriented attachment (OA), and Ostwald ripening (OR) mechanisms;[31] adapted with permission from ref 31. Copyright 2018 Springer Nature.

restriction of intramolecular motions of the M(I/II)−ligand complexes linked to the core, blocking nonradiative relaxation of excited states and thus activation of radiative pathways. At first, the M(I/II) precursor was converted into oligomeric M(I/II)−X complexes (X: carboxyl, thiol, chloride, hydroxyl, and amine groups), and then most of them reduced to M(0) nuclei by the reductive residues, i.e., tyrosine, tryptophan, and phenylalanine, in protein/peptide or bases, i.e., cytosine, in DNA. After that M(0) cores were sequestered by the M(I/II)−X complex shell due to a strong binding between M(0) and M(I/II), resulting in M(0)-on-M(I/II)−X intermediates. This is followed by slow aggregation into a M(0)NCs@M(I/II)L complex core−shell nanostructure by collision and fusion of M(0) atoms into an M(0) core and M(I/II)−X complex shell nanostructure (Figure 3A,B). For example, the AIE approach allows an intense orange-emissive biocompatible GSH-AuNC with large Stokes shift (>200 nm) and high QY (~15%) in a simple one-pot synthesis at pH ~ 7.[44] In the case of dual emissive Hb-AgNCs with large Stokes shift (>400 nm), both NC core oxidation and AIE mechanisms have contributed to the synthesis mechanism (pH ~ 12) (Figure 2A).[33] Moreover, the oriented attachment (OA) and Ostwald ripening (OR) phenomena together with the AIE mechanism can cause the growth of PtNCs and thus the formation of porous hollow luminescent nanotetrahedrons (Figure 3B). Notably, the AIE process can be accelerated with an increase in temperature (~60−70 °C), allowing a rather broad size distribution of PtNCs and even the self-aggregation and crystallization of nanotetrahedrons into porous and polycrystalline luminescent Pt microspheres (Figure 3B).[31] In another example, the AIE approach was achieved by changing pH (3.0 to 6.1) and subsequently by 5 h boiling, leading to highly fluorescent GSH-AgNCs with a core−shell Ag(0)@Ag(I)−thiolate nanostructure and three species, $Ag_{10}SG_6$, $Ag_{10}SG_5$, and $Ag_{11}SG_7$.[45] In this study, GSH-AgNCs were obtained with different sizes, while well-defined size GSH-AuNCs with high purity ($Au_{15}(SG)_{13}$) could be achieved in a controlled kinetic reduction reaction at pH ~ 2 together with the addition of borane *tert*-butylamine (TBAB) as a relatively weak reducing agent.[46] Moreover, the pH-controlled CO reduction approach causes GSH-AuNCs with well-defined sizes so that four discrete sizes of Au_{10-12}, Au_{15}, Au_{18}, and Au_{25} were obtained by adjusting the pH to 7.0, 9.0, 10.0, and 11.0, respectively, at a mole ratio of 2GSH/1HAuCl$_4$ at room temperature.[47] AIE can also be produced by controllable aggregation of the nonluminescent active metal complexes, e.g., Cu^1SR^1 ($R^1 = C_{10}H_{15}$), with inert metal Au^0 atoms, allowing the formation of Au_2Cu_6 nanoclusters with a high quantum yield of 11.7%.[48] The cleancap-regulated AIE is another strategy that has been confirmed for *p*-mercaptophenylboronic acid (MBA)-CuNCs. In this work CuNCs conjugate with glucose to connect with each other by the formation of the boronate esters between a pair of *cis*-diols on glucose and boronic acids of CuNCs. The hydrophobicity has been recently introduced as an effective parameter to induce the AIE nanoswitch for GSH-CuNCs by a trace amount of water in organic *N*,*N*′-dicyclohexylcarbodiimide (DCC) solvent[49] and for penicillamine-CuNCs by the removal of hydrophobic *p*-nitrophenol from the NC surface through α-cyclodextrin as a result of host−guest interaction.[50] The AIE strategy regulated by host−guest recognition has also been demonstrated for interaction between SH-β-cyclodextrin-CuNCs and hydrophobic di(adamantan-1-yl)phosphine as a connector.[51] Using a hydrophobic protecting ligand such as 4-methylthiophenol is another route to promote the AIE effect via hydrophobic interaction.[52] Altogether, we believe that these processes are dependent on the capping agent and metal species and synthesis conditions.

4. CAPPING AGENTS FOR COLORIMETRIC ASSAYS BASED ON FLUORESCENT NANOCLUSTERS

Capping agents are crucial when metal nanoclusters are used in colorimetry to detect specific analytes. The capping agent chosen is usually determined by the technique of synthesis, the nature of the nanoclusters, and the type of substances to be studied. Polysaccharides, peptides, proteins, amino acids, DNA, aptamers, polymers, small molecules, and dendrimers have all been used effectively as capping agents for metal nanoclusters used in colorimetric detection.[53] The following is a summary of the common capping agents that have been utilized in the production of metal nanoclusters to investigate potential new features and colorimetric assay uses.

4.1. Polysaccharides. Polysaccharides, as natural biomacromolecules, are gaining attraction in a variety of applications. They are stable, nontoxic, biocompatible, and biodegradable. They are easily available, cheap, and plentiful, and their hydrophilic functionalities can be used to target specific agents.[54] As an example, lentinan (LNT) is a bioactive polysaccharide with many hydroxyl groups which was used as a stabilizing and reducing agent to increase the dispersion of platinum nanoclusters (PtNCs). LNT-PtNCs provided many

https://doi.org/10.1021/acsomega.3c06884
ACS Omega 2024, 9, 3143−3163

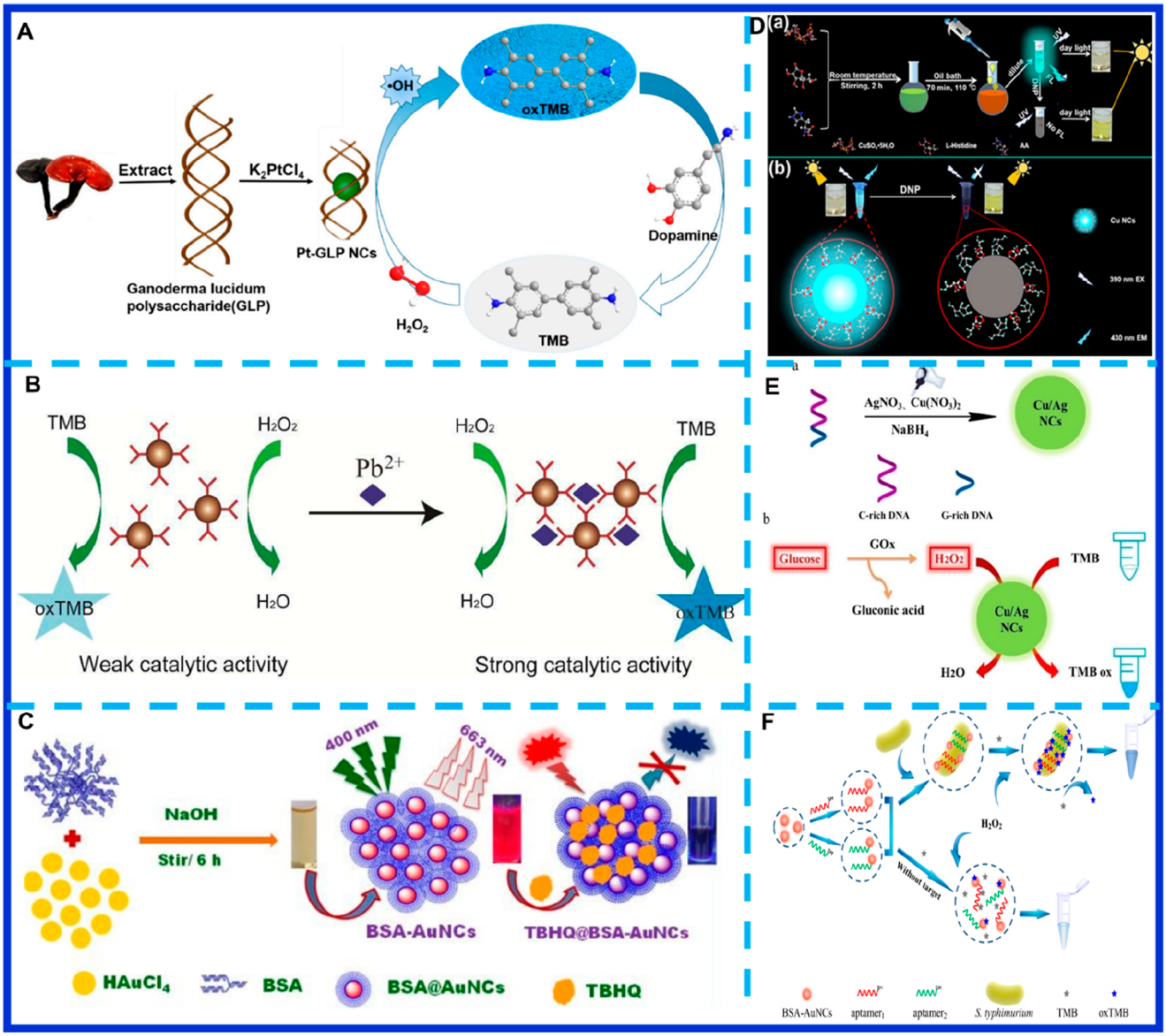

Figure 4. Examples of different stabilizing templates for the synthesis of FMNCs. (A) Polysaccharide: the synthesis of GLP-PtNCs for dopamine detection;[56] adapted with permission from ref 56. Copyright 2021 MDPI, under a CC BY 4.0 license. (B) Peptide: the aggregated GSH-AuNCs as a peroxidase-like mimic resulting in Pb^{2+}-induced accelerating oxidation of TMB by using H_2O_2;[65] adapted with permission from ref 65. Copyright 2017 Royal Society of Chemistry.(C) Protein: the synthesis of BSA-AuNCs for fluorometric and colorimetric detection of TBHQ and a color change solution as well as turn-off emission that happened as a result of a strong electrostatic interaction between TBHQ and NCs;[67] adapted with permission from ref 67. Copyright 2021 Royal Society of Chemistry. (D) Amino acid: (a) the synthesis of L-His-CuNCs and (b) DNP recognition by the inner filter effect (IFE) fluorescence mechanism (turn-off) and a new Meisenheimer complex formation allowing a color change to yellow solution;[69] adapted with permission from ref 69. Copyright 2021 IOP Publishing Ltd. (E) Nucleic acid: (a) the synthesis of NCs by cytosine-rich DNA in the presence of strong reducing agent ($NaBH_4$) and (b) its application for detection of H_2O_2 and glucose by peroxidase-like activity of DNA-Cu/AgNCs;[73] adapted with permission from ref 73. Copyright 2020 Wiley-VCH Verlag GmbH & Co. KGaA, Weinheim. (F) Aptamer: detection of *S. typhimurium* using aptamer@BSA-AuNCs based on the peroxidase-like activity enhancement of modified dual thiolated aptamers by bacteria in the presence of TMB and H_2O_2;[77] reprinted from ref 77. Copyright 2021 with permission from Elsevier.

catalytic active sites to increase H_2O_2 decomposition due to their ultrasmall size and stability. Lentinan molecules form hydrogen bond interactions in an aqueous solution, resulting in a stable triple helix conformation and catalyzing the oxidation of substrate TMB in the presence of H_2O_2 and providing a sensitive detection platform for glucose content in the urine samples of diabetic patients.[55] In another example, X. Lai et al. synthesized PtNCs using ganoderma lucidum polysaccharide (GLP). A helical conformation of GLP is formed by the presence of D-glucopyranosyl residues in the structure. Additionally, it contains many active groups, including hydroxyl and carboxyl groups. Nanoparticles wrapped in GLP were more stable because they were protected from aggregation. In the presence of GLP-Pt_{600}NCs, TMB was quickly catalyzed and oxidized to blue oxTMB due to the peroxidase-like activity of GLP-Pt_{600}NCs. Using this method, the LOD of dopamine (DA), an essential catecholamine neurotransmitter, was 0.66 μM with a color shift to clear blue. The method was also applied to detect DA in human serum samples with a recovery range of 96.66%−98.80% (Figure

https://doi.org/10.1021/acsomega.3c06884
ACS Omega 2024, 9, 3143−3163

4A).[56] K. Liu et al. also developed bitter gourd polysaccharide (BGP)-stabilized PtNCs with good cell biocompatibility and an extremely low hemolysis rate in colorimetric detection of ascorbic acid (AA). BGP's high stability and water solubility make it a suitable biological template for stabilizing metal nanoparticles. By reducing groups of BGPs, such as aldehyde groups, platinum ions can be reduced into Pt nanoparticles. These nanoparticles can be stabilized when soluble BGP is present. Within Pt-BGP NCs, PtNCs measure 0.83 ± 0.22 nm.[57] Chitosan (CS), another promising polysaccharide, has been regarded as a suitable material due to its exceptional properties such as biocompatibility, nontoxicity, biodegradability, and cost-effectiveness.[58] In this regard, Z. Dehghani et al. proposed a novel colorimetric sensor for tracing lead ions in milk samples based on Au/PtNCs and employing chitosan as a stabilizer. Based on the interaction of Pb^{2+} ions with chitosan functional groups and Au/PtNCs, adding Pb^{2+} causes chitosan-Au/PtNCs to aggregate, which results in size changes and decreases the enzymatic performance of Au/PtNCs. It was found that the recovery percentage ranged between 102 and 106%.[59]

4.2. Low-Molecular-Weight Thiols. Thiol-containing molecules of smaller size, including tiopronin, phenylethylthiolate, polyethylene glycol appended lipoic acid, and thiolate cyclodextrin, prove ideal for crafting NCs since they act as both reducing agents and capping ligands.[60−62] Recent studies uncovered that CuNCs synthesized using these low-molecular-weight thiols exhibit a unique property AIEE and amplify the emission intensity of the CuNCs.[49] However, AuNCs prepared with these thiols commonly exhibit lower QYs so that as the ratio of thiol-to-Au ions increases these particles tend to reduce in size, along with a decrease in their QY.[34] Glutathione (GSH) with potential in enhancing the fluorescence of NCs by managing their creation and stabilization is the most studied low-molecular-weight thiol peptide for the creation of FMNCs with excellent capability for colorimetric assay. GSH is a natural biocompatible thiol with the sequence g-Glu-Gly-Cys and good water solubility.[14] Under neutral conditions, GSH acts as a mild reducing agent and a strong capping agent, allowing partial reduction of Au ions to form AuNC cores, which could be stabilized by a thiolate−Au^+ complex. Employing a GSH-to-Au molar ratio (1.5:1) led to the production of fluorescent Au@Au^+-thiolate core−shell NCs through the controlled thiolate−Au^+ aggregation on the in situ formed Au cores, boasting a QY of around 15%.[63] Moreover, GSH-AuNCs have two free −COOH groups, one free $-NH_2$ group which is easily bonded with cations and the sulfhydryl functional group to ensure a firm bond with the precious metal surface. The thiol group within cysteine is also the active site within the GSH molecule, allowing it to interact with other molecules through thiol−disulfide exchange reactions. Taken together, among the above-mentioned thiol molecules, GSH-AuNCs with inherent peroxidase-like activity can be used for the ultrasensitive colorimetric detection. Q. Zhao et al. showed that this sensing platform employs a signal change, comprising a color change to dark green in an aqueous solution resulting from the presence of GSH-AuNCs and oxidized TMB which provides a visual colorimetric assay for H_2O_2 and glucose detection in serum samples.[64] H. Liao et al., in the second example, used a colorimetric approach for Pb^{2+} detection to demonstrate the increased peroxidase-like activity of GSH-AuNCs with Pb^{2+}-induced NC aggregation, resulting in an increased TMB oxidation by H_2O_2. Really, through GSH-Pb^{2+} interaction, GSH-AuNCs might form aggregates, resulting in aggregation-induced emission enhancement (AIEE), indicating a deep blue color. The Pb^{2+} recovery in the lake water ranged between 95.5% and 98.6% (Figure 4B).[65]

4.3. Proteins. Several functional metal nanomaterials have been created utilizing proteins like bovine serum albumin (BSA) as templates. BSA contains 582 amino acids with 35 threonines and 32 serines. BSA has numerous binding sites because it contains charged functional groups such as carboxyl, sulfhydryl, and amino. As a capping agent, BSA increases the bioavailability of nanoparticles loaded with nanoparticles by binding to these sites. Due to the presence of hydroxyl groups, BSA has mild reducing properties.[66] S. Shankar et al. described a colorimetric technique based on the strong electrostatic interaction between *tert*-butyl hydroquinone (TBHQ) as a kind of phenolic antioxidant and BSA-AuNCs. The addition of 50 μM TBHQ into BSA-AuNCs leads to a color change from colorless to dark brown. A range of 98.4−100.8% recovery was observed in edible and coconut oil samples (Figure 4C).[67] Keratin also contains multiple functional groups, including disulfide, amino, and carboxylic acids, particularly in the peptide backbone. S. Ma et al. prepared keratin-capped AuNCs with a peroxidase-like activity that can generate the oxTMB with H_2O_2. AuNCs were also modified with Cu^{2+} to enhance the catalytic activity and stability to be used for glucose colorimetric assay.[68]

4.4. Amino Acids. Among numerous amino acids, histidine with imidazole, amino, and the carboxylic acid group performs better with reducing ability. R. Xie et al. used L-histidine as a stabilizer and AA as a reducing agent to create luminous CuNCs in a simple one-pot method. The average diameter of the sizes was 3.3 ± 1.2 nm. Notably, CuNCs were a sensitive sensor capable of detecting 2,4-dinitrophenol (DNP). Histidine was used both as a template for CuNCs and as an electron donor group when it reacted with DNP, a proton-donating target. Notably, a new Meisenheimer complex formation through hydrogen bonding, acid−base pairing, and electrostatic interactions caused a yellow color change in the reaction solution from colorless. The recoveries in river water and tap water were found to be 91.2%−102% and 105.8%−114.7%, respectively (Figure 4D).[69] In another study, M. Fu et al. utilized His-AuNCs, which can catalyze the oxidation of colorless TMB for the detection of iodide (I^-) and Hg^{2+}. Increasing I^- concentration led to a color change from colorless to purple-red with high oxidase-like activity. Iodine atoms attached to nanocluster surfaces and promoted their aggregation. This platform with monodispersed clusters with a diameter of around 2 nm provides detection for I^- in serum samples.[70]

4.5. DNA. Both physical and chemical characteristics of DNA-templated metal nanoclusters are greatly impacted by the design of the DNA templates.[71] For example, DNA-Au/PtNCs were synthesized in a one-pot procedure for the sensitive detection of *Staphylococcus aureus* (*S. aureus*). In the presence of NCs, TMB, and H_2O_2, a color change was observed by adding *S. aureus*. The detection was further evaluated by a Y-shaped paper-based device. A range of 91.5%−100% recovery was observed for human serum, milk, and orange juice samples.[72]

Z. Du et al. synthesized Cu/AgNCs using DNA oligomers containing C-rich and G-rich sequences (c-myc TBA). The c-myc TBA-Cu/AgNCs indicated strong peroxidase activity by catalyzing colorless TMB to a blue product which was applied

https://doi.org/10.1021/acsomega.3c06884
ACS Omega 2024, 9, 3143−3163

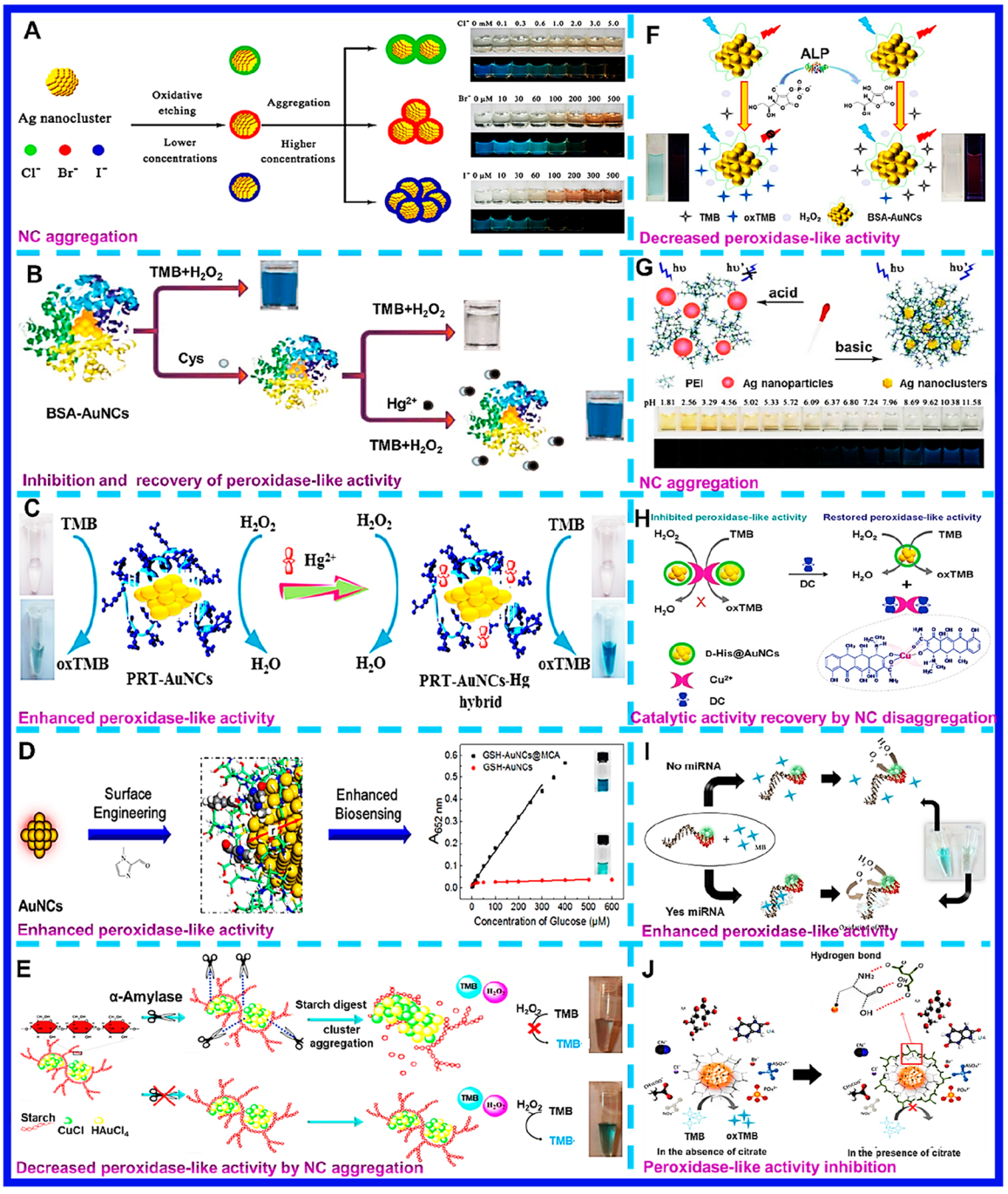

Figure 5. Examples of different target recognitions using FMNCs. (A) Detection of halide ions by PEI-AgNCs induced by oxidative etching and AgNC aggregation;[86] adapted with permission from ref 86. Copyright 2012 American Chemical Society. (B) Detection of Cys by inhibition of the peroxidase-like activity of BSA-AuNCs and Hg^{2+} recognition by restoration of the NC catalytic activity;[90] reprinted from ref 90. Copyright 2016 with permission from Elsevier. (C) The Hg(II) assay using peroxidase mimics PRT-AuNCs, and its activity increased selectively by mercury ions;[91] adapted with permission from ref 91. Copyright 2018 Springer Nature. (D) Surface engineering GSH-AuNCs as peroxidase mimics by 1-methyl-2-imidazolecarboxaldehyde (MCA) to enhance the sensitivity of glucose sensing in the presence of TMB and H_2O_2;[117] adapted with permission from ref 117. Copyright 2021 American Chemical Society. (E) α-Amylase detection by starch-Cu/AuNCs probes and TMB/H_2O_2 reagents based on the digestion of starch and thus cluster aggregation;[124] adapted with permission from ref 124. Copyright 2019 Springer Nature. (F) Dual-readout ALP assay based on the decreased peroxidase-like activity and fluorescence enhancement (turn on) of BSA-AuNCs;[130] reprinted from ref 130. Copyright 2019 with permission from Elsevier.(G) Designing a colorimetric PH sensor based on the aggregation of PEI-AgNCs with decreasing pH. Photographs of the color changes of AgNCs in Britton−Robinson (BR) buffers showing use of different pH values in the range of 1.81−11.58 under visible and UV lights;[131] adapted with permission from ref 131. Copyright 2013 American Chemical Society.(H) Sensitive assay of DC based on the restoration of peroxidase-like activity of D-His@AuNCs as a result of the strong coordination between DC and Cu^{2+} and thus the disaggregation of clusters;[146] adapted with permission from ref 146. Copyright 2020 Royal Society of Chemistry. (I) Detection of miR-155 by DNA-CuNCs based on the enhanced oxidation of methylene blue (MB) after intercalating into the DNA-CuNCs/miRNA-155 duplex;[157] reprinted from ref 157. Copyright 2018 with permission from Elsevier. (J) Citrate detection by the inhibited peroxidase-like activity of Cys-AuNCs;[169] reprinted from ref 169. Copyright 2019 with permission from Elsevier. The detection mechanism for each example is written in purple.

https://doi.org/10.1021/acsomega.3c06884
ACS Omega 2024, 9, 3143−3163

for selective detection of H_2O_2 and glucose. The recovery rate in serum samples was 95−103.3% (Figure 4E).[73] According to L.L. Wu et al., the addition of Hg^{2+} can inhibit the catalytic activity of Ag/PtNCs templated with a DNA sequence (CCCCCTAACTCCCCCTTTTTTTTTT). Incorporating both Hg^0 and Hg^{2+} interfered with the catalytic activity of DNA-Ag/PtNCs by aggregating them and decreasing the Pt^{2+} content on the DNA-Ag/PtNC surface. The device has the potential for detecting Hg^{2+} in tap water with a good recovery rate of 94.3−106.2%.[74]

4.6. Aptamers. Several aptamers have been demonstrated as potential colorimetric probes for different analytes that are difficult to detect with conventional probes.[75] It is noted that in these reports the aptamers have not been used as the NC stabilizer, while they are linked to the protein-stabilized AuNCs by thiol functional groups at 5′ or 3′ ends of DNA. For example, there have been a number of methods developed to detect food pathogens. The use of pasteurization and culture-based detection methods has not proven to be completely successful in controlling contamination in food. Enzyme-linked immunosorbent assays (ELISAs) are also costly and require a lot of biological reagents, which produces some false results. Additionally, polymerase chain reaction (PCR) requires complex instruments and sample preparation. Color change in pathogen samples is a simple way to detect pathogens using colorimetric biosensors. Using this method, Y. Song et al. synthesized aptamer@papain@AuNCs by entrapping Au in functional groups of a natural protease termed Papain. The thiolated aptamers were then used to react with these functional groups, such as −COOH. As a result of TMB adsorbing on bacteria surfaces, there is an increase in peroxidase activity to catch *E. coli* O157:H7. This sensor was able to successfully detect *E. coli* O157:H7 in ultrahigh temperature (UHT) sterilized, pasteurized, and raw milk. The prediscussed aptamer sequence was 5′-SH−CCGGACGCT-TATGCCTTGCCATCTACAGAGCAGGTGTGACGG-3′.[76] In another work, Q. Chen et al. developed aptamers@BSA-AuNCs for the selective detection of *Salmonella typhimurium* (*S. typhimurium*) using dual thiolated aptamers, BSA-AuNCs, and the TMB/H_2O_2 system. After the formation of Au−S bonds between BSA-AuNCs and both aptamers, microsized bacteria can capture both aptamers@BSA-AuNCs and TMB and so bring them both together, allowing a local increase in their concentration. Based on the enhanced peroxidase-like activity of this designed aptasensor coupling with *S. typhimurium* in the presence of TMB and H_2O_2, a color change from light blue to dark blue was reported. Eggshell and egg white samples were also used to successfully validate the results, and the recovery ranged from 92.4% to 110% (Figure 4F).[77]

5. APPLICATIONS

5.1. Ion Detection. Abnormality in ion levels may cause serious harm to humans and the environment which highlights the importance of ion detection. Heavy metal ions (e.g., Hg^{2+}, Cr^{6+}), having distinct properties, such as high toxicity, high bioaccumulation, non-natural breakdown, and convoluted sources, harm the environment and human health. Halides, nitrites, and phosphates are examples of inorganic anions that can be advantageous or harmful depending on their concentration.[78] Although numerous determination techniques may be utilized, such as ion chromatography (IC),[79] electrochemical characterization,[80] atomic absorption spectrometry,[81,82] inductively coupled plasma mass spectroscopy (ICPMS),[83] inductively coupled plasma atomic emission spectrometry (ICP-AES),[84] their time consumption, high cost, and laborious sample preparation processes have limited their applications.[85] Regarding this, colorimetric assays based on the different ions including halides, heavy metal ions, nitrite, and sulfide ions using noble metal nanoclusters (AgNCs, AuNCs, CuNCs, and bimetallic NCs) have been classified.

5.1.1. Halides. F. Qu et al. utilized PEI-AgNCs to provide a colorimetric platform for the sensitive identification of halide ions. Interaction between Ag atoms of PEI-AgNCs and halides in addition to the formation of larger particles provides the foundation for detecting halide ions. The colorless solution turned yellow by adding Cl^-. Increasing the concentration of Br^- gave a color change into brown, while adding I^- turned the solution to dark brown. It demonstrates that the high affinity between Ag−halide bonds and the low solubility product constant (K_{sp}) of silver halide compounds can result in oxidative etching and aggregation of silver nanoclusters (Figure 5A).[86]

5.1.2. Heavy Metal Ions (Hg^{2+}, Pb^{2+}, Cr^{6+}, and Fe^{2+}). By utilizing AgNCs with poly(acrylic acid), Y. Tao et al. also created a colorimetric probe indicating a color change from purple to pale red by the addition of Hg^{2+} ions with an enhancement in the absorption peak at 510 nm and a LOD of 5 nM.[87] Several reasons have contributed to the current interest in AuNCs, including their biocompatibility, ultrafine size, photostability, and fluorescence properties.[2,88] Unlike CdSe, CdTe, PbS, etc., AuNCs contain no harmful heavy metals. Meanwhile, AuNCs are also more stable than AgNCs due to gold's enhanced oxidation resistance.[89] Using the one-pot method, Y. W. Wang et al. demonstrated a new colorimetric assay for the detection of cysteine and Hg^{2+} in an aqueous solution within 10 min. BSA-AuNCs were synthesized and performed catalytic activity. The catalytic reaction was carried out using Cys as an inhibitor. SH groups of cysteine interact with Au atoms. Furthermore, the addition of Hg^{2+} recovers the catalytic activity of BSA-AuNCs. As a result of the high affinity of thiolates toward Hg^{2+}, thiols broke away from AuNC surfaces, resulting in the breakage of the Au−SH bond. This results in a color change to blue produced by Hg^{2+}-induced recovery of the catalytic activity of the BSA-AuNCs (Figure 5B).[90] Protamines as low-molecular-weight basic proteins with high arginine content can deliver the DNA to the nucleus of the egg. Y.Q. Huang et al. used protamine to synthesize AuNCs under the one-pot method. The developed PRT-AuNCs exhibited peroxidase-like activity toward Hg^{2+}. Significantly, Hg^{2+} could dramatically and selectively increase the peroxidase-like activity of AuNCs. The enhanced mechanism induced by Hg^{2+} was related to the Hg^{2+}−Au^0/Au^+ interaction, generating the partly oxidized Au ($Au^{\delta+}$) and the cationic Au species. Moreover, the designed colorimetric method is highly sensitive (LOD = 1.16 nM) with a wide linear range. The recovery was assayed in water samples ranging from 99.81% to 102.9% (Figure 5C).[91] Moreover, test strips by Wang et al. were designed based on using 4-chlorothiophenol-protected CuNCs. This sensing platform can be used to detect Hg^{2+} with self-assembly-induced emission (S-AIE) CuNCs which may lead to a color shift from red to blue-purple. The platform has also been utilized for the detection of Hg^{2+} in tap and lake water samples with a recovery of 98.3−103.0%.[92] By incorporating a secondary metallic element into metal NCs,

https://doi.org/10.1021/acsomega.3c06884
ACS Omega 2024, 9, 3143−3163

enhanced catalytic activity can be achieved with high selectivity and improved thermal stability. The geometric and electrical structures, the atomic distribution of reactive metals, the electron-donating action of capping ligands, and the type of support have all been found to be strongly related to total catalytic performance.[93] Recently, attempts have been made to apply the bimetal NCs for colorimetric assay. In this regard, Y. Cai et al. developed bimetallic GSH-Ag/CuNCs by biomimetic mineralization using GSH and $NaBH_4$. Due to the high affinity between GSH and Hg (Hg−S) bonds, and also Ag−Hg and Cu−Hg bonds, strong peroxidase-like activity was achieved, and the color change to dark blue in the presence of Hg^{2+} provided a colorimetric technique with a good linear range (0.1−700 nM) and a LOD of 0.05 nM. Real samples including seawater, urine, human serum, and mineral water showed a recovery rate of 96% to 104%.[94] As reported by R. Liu et al., metallothionein (MT)-CuNCs were able to convert catalase-like activity into peroxidase-like activity when exposed to lead and mercury ions. In MT-CuNCs, the interactions between Pb^{2+}/Hg^{2+}, Cu/Cu^{+}, and MT influence the coordination bonds. In the presence of TMB and H_2O_2, Pb^{2+} and Hg^{2+} caused a color change from colorless to dark blue. Therefore, this system could be applied to detect heavy metals in tap water, pond water, and river water.[95] Polyethylenimine (PEI)-capped AgNCs are also attractive in many applications. As an example, Q. Xue et al. synthesized PEI-AgNCs with oxidoreductase-like catalytic ability to detect Cr^{6+} when reacting with the TMB in pH 3.0, demonstrating a color change to light blue providing colorimetric analysis of Cr^{6+} with a LOD as low as 1.1 μM.[96] Poly(methacrylic acid)-capped AgNCs were employed by K. Chaiendoo et al. in a one-pot reaction. With a LOD of 76 nM within a linear range of 5−100 μM, the PMAA-AgNCs demonstrated selective Fe^{2+} detection over other cations with an orange color change. Fe^{2+} can reduce unreacted Ag^{+} in AgNC solutions to Ag^{0}, which in turn deposits on AgNCs and increases particle size.[97]

5.1.3. Nitrite Ions. L. Liu et al. reported that His@AuNCs/RGO exhibited stronger oxidase mimetic activity in comparison with BSA@AuNCs, Cyt@AuNCs, and Lys@AuNCs. This may be caused by AuNCs, imidazole groups in histidine, and reduced graphene oxide (RGO) working synergistically to enhance electron transfer from catalytic active sites. Really, in this work to improve catalytic and electrocatalytic activity, His@AuNCs were coupled with RGO by electrostatic forces. Adsorption of nitrite on His@AuNCs/RGO inhibited the oxidation of the TMB substrate. This allows selective detection of nitrite ions by which the color changes happen from light yellow to light brown. There was a range of 94.67%−100.28% recovery in sausage samples.[98]

5.1.4. Sulfide Ions. Comparatively, there is a smaller number of reports about CuNCs than AuNCs and AgNCs for sulfide ion detection, even though they are cheaper and more available. Z. Shojaeifard et al. created tannic-acid-capped CuNCs with Cu^{2+} ions for the detection of sulfide ions. Increasing the concentration of sulfide between 6.0 and 130.0 μM turned the color of the blue solution to brown due to the formation of CuS. Ta-CuNCs/Cu^{2+} could enhance the peak absorbance at around 350−500 nm. The water samples showed a recovery value of 96.15−103.82%.[99] Also, taking advantage of the peroxidase-like activity of GSH-CuNCs, H. Liao et al. presented a colorimetric assay to detect sulfide ions with an LOD of 0.5 μM. It should be considered that the maximum inhibition effect of sulfide ions on the catalytic activity of NCs was obtained at pH 4.0. Sulfide ions are strongly associated with Cu(I) on the surface of CuNCs, thereby significantly affecting the conversion of H_2O_2 to OH· radicals. The results were also validated via real samples. For tap water, the recovery of sulfide ions ranged from 97.6 to 98.9%, and for lake water, it ranged from 93.8% to 96.3%.[100]

5.2. Small Molecules. The detection of small molecules has been used for many purposes, including diagnosis, medicine, environmental sampling, food, and agricultural assessment. In addition, the identification of small molecules as regulatory factors plays an important role in the diagnosis of different diseases. The liver metabolizes bilirubin to excrete it from the body after it is produced by the catabolism of hemoglobin in red blood cells. Hyperbilirubinemia, also known as jaundice, results from a high level of bilirubin in the blood, resulting in a yellow coloration of skin and tissue.[101] Toward diagnosis of jaundice, R.S. Aparna et al. used BSA-CuNCs as the colorimetric probe for the detection of bilirubin. The copper−bilirubin complex resulted in a clear color change from pale pink to green which facilitated the colorimetric detection of bilirubin.[102] Nitrophenols as other important small molecules are used in dye industrial processes, pharmaceuticals, and chemistry. They are still present in the soil and groundwater as organic compounds, causing harm to wildlife and humans. To detect *p*-nitrophenol, F. Qu et al. created PEI-AgNCs with various terminal groups. It was determined that the production of the oxygen anion of *p*-NP, which was caused by the transfer of H+ from *p*-NP to the amine groups of PEI, was the cause of the color change from light yellow to deep yellow after the addition of *p*-NP.[103] Y. Du et al. synthesized a mercaptosuccinic acid (MSA)-CuNC without using any chromogenic reagent. Due to the aggregation of the CuNPs and the valence transition of Cu, a color change from red to yellow was observed by the addition of H_2O_2, a critical product in essential biological processes. For tap water samples, recoveries ranged from 96.7% to 104.1% for the determination of H_2O_2.[104] In continuation of the discussion, a high level of xanthine as an animal metabolic product can cause gout, uric acid deposits, and renal calculi since it can be oxidized to uric acid. Z. Yan et al. used dithiothreitol and BSA to create new CuNCs for detecting xanthine. The absorbance intensity of the TMB/CuNC system at 652 nm increased with 0.5 μM xanthine in the presence of 5 M of different interferences based on the peroxidase-like activity of CuNCs. Because xanthine oxidase may catalyze the oxidation of xanthine to release H_2O_2, an indirect approach for detecting xanthine was developed. There is a recovery rate of 90.2%−93.1% for the detection of xanthine in serum samples.[105] In many biological processes, pyrophosphate (PPi) is generated by the hydrolysis of nucleoside triphosphates. Chondrocalcinosis, urolithiasis, and cancer have all been linked to high PPi levels in urine and synovial fluid. Y. Shi et al. demonstrated a very sensitive colorimetric approach for quantifying PPi via the AuNCs-Cu^{2+} system together with significant catalytic activity in the TMB-H_2O_2 system. However, the catalytic activity of AuNCs-Cu^{2+} reduced in the presence of PPi because the affinity between Cu^{2+} and PPi was greater than that between Cu^{2+} and AuNCs. In human urine samples, recovery of PPi ranged from 94.95 to 100.79%.[106] It is also important to detect AA in a variety of biochemical and pharmaceutical processes due to its antioxidative properties. X. Yang et al. suggested a colorimetric technique using BSA-AgNCs to detect AA in the range from 2.0 to 50.0 μM, with the corresponding LOD of 0.16 μM.

https://doi.org/10.1021/acsomega.3c06884
ACS Omega 2024, 9, 3143−3163

Using BSA-AgNCs, silver nanoparticles were formed uniformly, while the color of the solution changed to yellow via reducing Ag^+ to Ag^0 by ascorbic acid.[107]

As a result of their high cost and rarity, PtNCs have been limited in their applications despite their enzyme-like activity. In order to make the best out of it, N. Qiu et al. employed the electrodeposition technique with cetyltrimethylammonium bromide (CTAB) to graft three-dimensional graphene foam (3D GF) onto PtNCs. Based on the inhibition effect of this novel recyclable nanohybrid with hydroquinone (HQ), a harmful pollutant, colorimetric detection of HQ with a LOD of 76 nM, was achieved. By increasing the concentration of HQ, the color change reaction became weaker. In addition to TMB, other substrates such as ABTS, catechol, and L-DOPA also showed a high oxidase-like catalytic activity with a 3D GF-PtNC nanohybrid.[108]

5.3. Glucose Detection. The value of fast and simple detection of glucose in human fluid, especially in blood, is very important for metabolic diseases like diabetes. So, a quick, precise, and sensitive detection method is needed.[55,109,110] For blood glucose determination, several analytical methods have been developed, including surface-enhanced Raman scattering,[111] electrochemistry,[112] fluorescence,[113] chemiluminescence,[114] and spectrophotometry.[115] Common methods have several disadvantages, such as their inherent difficulty in purification as well as their poor stability.[116] In this regard, F. Sun et al. demonstrated that 1-methyl-2-imidazolecarboxaldehyde (MCA) could have a high potential application for glucose sensing in serum samples by using the peroxidase-like catalytic activity of GSH-AuNCs in oxidizing TMB which increased in the presence of H_2O_2. By oxidizing glucose in the presence of oxygen, glucose oxidase (GOx) is capable of generating gluconic acid and H_2O_2. As a result of weak interactions of MCA, MCA can penetrate through the layer of GSH and thus locate near the surface of AuNCs. In the presence of H_2O_2 due to glucose oxidation, the solution color turned from light blue to deep blue mainly due to more produced oxTMB in the solution (Figure 5D).[117]

J. Chi et al. developed a colorimetric system with an improved peroxidase-like activity using Au, GOx, and zeolitic imidazolate frameworks (AuNCs@ZIF-8) which could detect glucose by the produced H_2O_2 from the reaction between glucose and GOx.[116] J. Feng et al. fabricated gold−platinum nanoclusters with an optimal Au/Pt molar ratio (1:1) by a one-pot synthetic route. The NCs-GOx cascade-catalyzed system using TMB enabled sensitive and selective glucose detection. This assay can be used not only for the visual detection of glucose but also for convenient and reliable quantification in the concentration range of 5.0−55 μM with an LOD of 2.4 μM.[118] In the same way, H. Sun et al. synthesized Au-PtNCs with guanosine monophosphate (GMP). In the presence of glucose, the colorless *o*-phenylenediamine (OPD) was oxidized to yellow 2,3-diamino phenazine (DAP). The linear range of the colorimetric method toward glucose was in the range of 0.05−0.4 mM, with an LOD of 11 μM. In human serum samples, recoveries ranged from 98.30% to 100.27%.[119] L. Jin et al. synthesized ultrasmall PtNCs using yeast extract through a facile one-pot approach. The yeast extract-stabilized PtNCs possess excellent water solubility as well as attractive peroxidase-mimicking properties, which caused them to be used as a sensitive colorimetric method for glucose detection. The LOD was achieved as low as 0.28 μM, and the recovery of the designed probe in serum samples ranged from 96.1% to 101.5%.[120] In conclusion, these rapid, accurate, and reliable sensing platforms can be used to visualize glucose in human serum directly, with no reagents or instruments.

5.4. Macromolecules. Colorimetric assays for macromolecules like proteins have been mostly limited to enzyme detection. Heparin is a highly sulfated glycosaminoglycan used in anticoagulation procedures. L. Hu et al. demonstrated that heparin accelerated the peroxidase-like activity of AuNCs at neutral pH. However, heparinase hydrolyzed heparin into small fragments, which minimized the catalytic enhancement effect. This led to colorimetric heparinase measurements with an LOD of 0.06 $\mu g \cdot mL^{-1}$. Using diluted fetal bovine serum, recovery rates ranged from 95.3% to 97.0%.[121] Thrombin plays a crucial role in repairing injured vessels. The effects of thrombin as a protein activating multiple receptors on cancer cell migration, vascular diseases, and Alzheimer's disease have been suggested by research results.[122] C. Zheng et al. utilized a one-step approach to synthesize Ag/PtNCs with a C-rich DNA template exhibiting peroxidase-like catalytic activity, coupled with a thrombin aptamer, leading to a color change to yellow. This aptamer-based sandwich-type strategy was utilized to detect thrombin concentrations as a coagulation factor in the range from 1 nM to 50 nM, allowing an LOD of 2.6 nM.[123]

Researchers have found that blood levels of the α-amylase enzyme are higher in salivary gland inflammation and acute pancreatitis, and it is also effective in controlling type 2 diabetes mellitus. Another work represents the detection system of this enzyme that utilizes the interaction of α-amylase with starch-supported Au/CuNCs. The α-amylase diagnosis mechanism is based on the starch digestion by α-amylase in the presence of TMB and H_2O_2, which results in nanocluster aggregation, allowing an increase in the nanoparticle size and thus a decrease in the peroxidase-like activity of the Cu/AuNCs. Using this system, sensitive colorimetric sensing of α-amylase was achieved with an LOD of 0.04 U/mL, and good recoveries ranged from 94.5% to 103.1% in serum samples (Figure 5E).[124] Trypsin is one of the digestive enzymes that is employed in food technology as well as in the diagnosis of pancreatitis and cystic fibrosis.[125] G. Wang et al. demonstrated that trypsin can digest the protein template of BSA-AuNCs and inhibit the catalytic activity of BSA-AuNCs. As a result of a change in surface state and aggregation of AuNCs after the digestion of BSA, a colorimetric assay with an LOD of 0.6 g/mL was performed to detect trypsin with a wider linear range compared to other methods.[10] Matrix metalloproteinases (MMPs) are proteolytic enzymes whose overexpression may indicate cancer. To detect MMPs, M. Dadmehr et al. developed AuNPs@gelatin/AuNCs by depositing gelatin/AuNCs on AuNPs. In the pH range of 4−12, increasing MMP-9 concentration results in a visual color shift from red to purple. The as-prepared sensor was successfully applied to serum samples, with recovery percentages of 95%−108%.[126]

5.5. Enzyme Activity Assays. As a significant enzyme in human body tissues, ALP concentration ranges between 25 and 100 IU/L. When the concentration reaches 300 IU/L, it indicates liver, bone, and cancer diseases.[127] The hydrogenation catalyzed by ALP is often detected by electrochemical and spectroscopic methods. The development of a high-resolution colorimetric procedure to induce a noticeable color shift would be appreciated.[128,129] Based on the peroxidase-mimicking activity of BSA-AuNCs, P. Ni et al. developed a colorimetric technique that was employed to detect ALP activity. The hydrolysis of L-AA-2-phosphate in the presence of

https://doi.org/10.1021/acsomega.3c06884
ACS Omega 2024, 9, 3143−3163

ALP produces AA, which can inhibit the oxidation of TMB. This phenomenon was observed by a color change from dark blue to light blue and a decrease in absorbance at 652 nm. The recovery rates in human serum samples ranged from 101.0% to 120.5% (Figure 5F).[130] However, more studies are required to utilize NCs for developing enzyme activity sensors.

5.6. pH Sensor. It is well-known that pH plays an important role in biochemical processes, particularly in the metabolism of adenosine triphosphate (ATP). Nanoclusters introduce new possibilities for designing pH sensors because of their unique features. However, only a few studies have investigated the pH-responsive optical properties of nanoclusters so far. According to F. Qu et al., PEI-AgNCs are the only NCs that can act as pH sensors because of their charge distribution and amino groups. In addition to reacting quickly to pH changes, it also exhibits absorption properties that change from almost colorless to colored as the acidity increases, so it could be used as a color indicator for pH detection in physiological environments ranging from 5.0 to 7.4. With lowering pH, the repulsion development and structural change of PEI drive AgNC aggregation, resulting in an evident color shift (Figure 5G).[131] There is a need for further research into pH sensing using colorimetric nanoclusters, as this report was the only one that employed this method.

5.7. Biomarker Thiols. Thiols are biochemically active components of the sulfur cycle in nature. Cystine (Cys) and glutathione (GSH) are examples of low-molecular-mass thiols that are crucial cellular components in the processes of metabolism and homeostasis in physiological fluids, including plasma and urine, as well as a variety of pathological and physiological functions.[132,133] As an amino acid that contains sulfur, cysteine facilitates the formation of disulfide bonds that stabilize the secondary structures and functions of proteins. Besides being a biomarker, it may also play a role in cancer biology as a physiological regulator.[134] Thus, many techniques have been developed to detect cysteine and GSH, including fluorescent methods,[135,136] electrochemical methods,[137] and high-performance liquid chromatography (HPLC).[138] Since these techniques are complex, developing simple assays is important. In this regard, X. Yuan et al. developed GSH-AgNCs. The GSH layer on the AgNC surface caused the differentiation of Cys from other large-sized thiol molecules (e.g., GSH) simply by their size. The high affinity of the thiol−Ag interaction and the small size of GSH-AgNCs provided high sensitivity for Cys detection. Under visible light, unlike the other 19 amino acids, GSH-AgNC solution with cysteine was colorless.[139] J.J. Li et al. improved the catalytic activity of GSH-AuNCs with Pt as the second metal content via a one-pot approach. In this case, Cys could selectively and efficiently inhibit the peroxidase-like activity of GSH-Au/PtNCs, allowing a decrease in the absorption intensity at 652 nm as an abstract of the decrease in the ox-TMB, and color changes from blue to colorless in the presence of cysteine with a linear range from 0.5 to 30 μM. Accordingly, the recovery rates for artificial urine and serum ranged from 97.86% to 102.42% and 96.50% to 101.42%, respectively.[140]

GSH as a critical biothiol has multiple functions in cells, including protecting the cells from oxidative stress by trapping free radicals.[141] Research has shown that cancer cells have a GSH content four times greater than normal cells.[142] Hence, creating an analytical technique that detects GSH quickly, accurately, and consistently is key. Here are some examples of unique and simple methods for colorimetric GSH level measurement based on the inhibitory impact of GSH on the peroxidase-like activity of NCs. J. Feng et al. developed GSH-AuNCs which were used for the detection of GSH in the presence of TMB and H_2O_2, indicating a colorimetric assay by inhibition of the peroxidase activity with an LOD of 420 nM. The assay was also evaluated for the supernatant of human normal cells and cancer cells. Compared to normal cells, cancer cells had a much higher level of GSH.[143]

Based on the peroxidase activity of CuNCs, prepared cysteamine, and hydrazine hydrate, C. Liu et al. developed a sensitive colorimetric assay toward GSH with an LOD of 0.89 μM.[144] C. Jiang et al. presented a label-free sensing assay for the colorimetric detection of GSH, glutathione reductase (GR), and glutathione oxidized (GSSG) based on the enzyme-mimicking characteristic of cytidine-AuNCs. The interaction between GSH and Cy-AuNCs at the surface led to the inhibitory effect providing another selective platform for the detection of biothiols.[145]

5.8. Drugs. A colorimetric assay is a useful tool for controlling the overdose of drugs by detecting the level of the drugs. As a widely used commercial antibiotic, doxycycline (DC) is widely used in human infections. Human fluids should therefore be screened for DC levels sensitively and selectively to prevent ineffective treatment and side effects. For DC colorimetric detection, Y. Song et al. synthesized the D-histidine-stabilized AuNCs and applied them for the promotion of hydrogen peroxide in the catalytic oxidation of TMB. The restoration of the enzyme-mimicking catalytic activity of D-His@AuNCs happens with the addition of doxycycline, based on strong coordination between Cu^{2+} and doxycycline. Really, unlike other analytes, D-His@AuNCs could be selectively complexed with Cu^{2+} via carboxylate and amino groups of His, resulting in NC aggregation and the color change from bright blue to light blue, but then the solution color could be recovered to dark blue due to the Cu^{2+}/DC complex formation and thus the disaggregation of clusters. This showed a strong linear relationship in a concentration range of the doxycycline with an LOD of 1.0 μM (Figure 5H).[146] Z. Zhang et al. improved the catalytic activity of AuNCs together with selectivity using aptamers (Apt) and developed a colorimetric sensing platform for the detection of tetracycline antibiotics (TCs). This sensing apparatus can detect TCs in the range of 1−16 μM with an LOD < 46 nM due to the conformational change of Apt with TCs resulting in a blue solution. In general, the proposed aptasensor has a recovery rate of 96.0−105% for TCs.[147] Further, Q. Zhao et al. have noted that the detection of abused drugs such as methamphetamine (MA) is one of the most critical issues to address. In this work, the reaction between the antibody-immobilized polystyrene plate and AuNC-conjugated antibodies created a color change.[148] Nevertheless, colorimetric drug detection faces many challenges due to its low sensitivity.

5.9. Nucleic Acids. Considering the importance of nucleic acid detection in diagnostic applications, there are several approaches for the detection of nucleic acids, including electrochemical methods,[149,150] spectrometry,[151] CRISPR-Cas systems,[152] and fluorescent-based methods,[153] that mostly required amplification using polymerase chain reaction (PCR) before detection.[154] Since their instruments are expensive and they need highly skilled people, developing simple and fast biosensing systems is crucial. MicroRNAs (miRNAs) are noncoding RNAs found that play important roles in regulatory

https://doi.org/10.1021/acsomega.3c06884
ACS Omega 2024, 9, 3143−3163

functions and disorders and may potentially be used as a screening biomarker for cancer detection.[155] As a result, finding innovative tools for the rapid, accurate, and sensitive detection of miRNAs is an important field of research. The expression of miRNA-21 is a reliable biomarker for early cancer detection. Based on DNA-Ag/PtNCs, which can catalyze the reaction between H_2O_2 and TMB, N. Fakhri et al. developed a paper-based biosensor for detecting sub-micromolar amounts of miRNA-21. By inhibiting peroxidase-like activity, miRNA-21 could be detected linearly in the 1−700 pM range with an LOD of 0.6 pM. A paper assay was also conducted using a Y-shaped paper-based microfluidic device to take advantage of the special features of microchannels, like quick reaction times, low reagent volumes, and affordable fabrication costs. The LOD was 4.1 ppm, and the linear range was 10−10000 pM.[156]

As an electrochemical and colorimetric indicator, MB is a positively charged aromatic organic dye that intercalates into double-stranded DNA by $\pi-\pi$ interactions. As a result of the CuNC peroxidase catalytic reaction, O_2 is generated as a byproduct. Once MB is intercalated into a duplex, oxidation of MB by O_2 is greatly enhanced. A colorimetric platform based on MB oxidation and the hybridization effects of miRNA-155 with DNA-CuNCs without enzymes or other primers have been developed for the detection of the oncogenic miRNA-155 which is a breast cancer biomarker. As a result of adding miRNA-155 in the range of 1.0 pM to 10.0 nM, MB interacts with dsDNA/miR-155, and this interaction decreases the absorbance signal of the MB. This detection assay for serum, which has a 99% recovery, provides an early diagnosis and a prognosis assessment of breast cancer (Figure 5I).[157] According to Z. Dehghani et al., a colorimetric DNA biosensor using Au/PtNCs synthesized by a cytosine-rich DNA sequence was developed in the presence of TMB and H_2O_2. The detection of the *Campylobacter jejuni* DNA genome as a pathogenic bacteria was their main issue. Since the DNA probe Au/PtNCs did not hybridize with noncomplementary DNA, the structure of the biosensor remained intact, and the peroxidase-like activity remained. When DNA-Au/PtNCs were used against perfectly matched DNA, their blue color intensities were much lower than when they were applied to mismatched DNA. By reducing the peroxidase activity in Au/PtNCs by hybridization with DNA, this technique is based on the principle of DNA−DNA hybridization. The LOD was 20 pM in the presence of target DNA.[158]

5.10. Cancer Cell Detection. Although cancer is one of the most common causes of disease in the world, an early diagnosis can significantly improve the outlook and prognosis of the patients. This means that the detection of cancer cells and biomarkers could enhance the chances of successful therapeutic intervention and recovery from cancer. However, most cancer detection methods require advanced instrumentation and are time and cost-consuming.[12] There are some techniques used to make point-of-care diagnoses. However, colorimetric assays are highly popular because of their low cost, providing direct visualization, simplicity, and rapid results.[159−161] Many different "signals" (e.g., proteins, nucleic acids, exosomes, etc.) released by cancer cells have been discussed, and the accurate and specific identification of them is significant for cancer patients' early diagnosis and treatment.[142]

5.10.1. Breast Cancer. The successful development of sensitive sensors for breast cancer cell detection is crucial for breast cancer diagnosis since breast cancer is the most prevalent malignancy and a major cause of mortality in women worldwide.[162] Human epidermal growth factor receptor-2 (HER2) can be amplified in aggressive breast cancers.[163] Y. Tao et al. produced AuNCs-loaded liposomes (AuNCs-LPs) that performed peroxidase-like activity through the extrusion method, and AuNCs-LPs after functionalization with ErbB2/Her2 antibodies (anti-Her2) could detect SKBR3 and MCF7 breast cancer cell lines, expressing HER2 by recognizing the HER2 receptor on the cell surface. After the addition of SKBR3 cells in the presence of BSA-AuNCs-LPs-anti-HER2, color changes to deep blue were observed with TMB/H_2O_2. In the presence of a target cell population ranging from 5 to 1000 cells, the absorbance of TMB at 652 nm linearly increased, with a low LOD of five cells.[164] M. Li et al. reported efficient detection of HER^{2+} breast cancer cells with a LOD down to 10 cells using mesoporous silica (MSN)-AuNCs. Having low toxicity, high surface area, high pore volume, and unique morphology, MSN provides excellent enzyme immobilization support for AuNCs-anti-HER2 with a peroxidase-like property that catalyzes the oxidation of TMB by H_2O_2.[165] Having a large surface area (~2630 m^2 g^{-1}) and functional groups, graphene oxide (GO) has been used as a nanohybrid biosensing platform.[42] Y. Tao et al. designed GO-AuNCs hybrids with high catalytic activity over a broad pH range by absorbing AuNCs on GO via electrostatic interactions to regulate lysozyme-AuNCs' peroxidase-like activity. In order to improve cancer targeting, FAGO-AuNC hybrids (GFA) can be used with the conjugation of AuNCs with folic acid (FA). A color reaction would be catalyzed by GFA-conjugated cells in the presence of TMB and H_2O_2, monitored by changes in absorbance at 652 nm. There was a significant change in absorbance as the number of MCF-7 cells increased, which suggested that a greater amount of GFA was bound to folate receptors on the surface of MCF-7 cells. As a result of using this method, the LOD was as low as 5 cells.[12]

5.10.2. Prostate Cancer. It is significant to note that prostate cancer is the most common cancer among men in the United States. However, if detected early, it has a high survival rate.[166,167] Current prostate cancer diagnostic methods are invasive and do not detect aggressive forms of the disease.[168] S. Abarghoei et al. designed a colorimetric technique using Cys-AuNCs as a peroxidase mimetic for the detection of citrate as a biomarker for the early stage detection of prostate cancer. Citrate has hydroxyl and carboxylic groups that can easily bind with free carboxyl and free amino groups of cysteine via hydrogen bonds, thus creating a shell on the surface of the AuNCs and inhibiting the oxidation activity of the cluster. Accordingly, a broad linear relationship for citrate was achieved for the range of 0.5−1000 μM. The LOD of the proposed method was obtained as 0.1 μM. A recovery rate of 86.0%−98.0% was obtained with the present biosensor ($n = 3$), which indicates a promising result as it shows that citrates are precisely detectable in urine samples (Figure 5J).[169]

6. SUMMARY, CHALLENGES, AND FUTURE

An acceptable number of colorimetric detections exist based on fluorescent metal nanocluster probes, including the detection of ions, amino acids, peptides, small molecules, macromolecules, enzyme activity, pH, and cancer cells. FMNCs are capable of catalyzing the substrate to generate a color change that could be directly observed by the naked eye. The difficult parameters in a colorimetric assay to handle

https://doi.org/10.1021/acsomega.3c06884
ACS Omega 2024, 9, 3143−3163

would have high sensitivity and specificity, rapid reaction detection, stability, and biocompatibility. In spite of such above-mentioned discoveries, several critical challenges in this field need to be addressed as follows: (i) The only pH-sensitive nanocluster reported so far (PEI-AgNCs), and so developing colorimetric pH sensors based on FMNCs can be extended. (ii) Moreover, there are no reports regarding the colorimetric assay using aptamer-stabilized NCs, and few related works show the efficacy of the thiolated aptamers in the presence of protein-stabilized AuNCs. (iii) Despite the relevance of amino acids as metabolite biomarkers in disease diagnosis, including sarcosine, alanine, leucine, histidine, and proline,[170] etc., the colorimetric detection of amino acids using FMNCs has been confined to cysteine. (iv) Furthermore, cancer diagnosis based on nanocluster probes by the colorimetric method have been limited to breast and prostate cancers without any real or clinical sample reports. (v) The detection of viruses is a topic that has been less discussed in colorimetric assays using metal nanoclusters which highlights the shortcomings of the current works for viral disease diagnostics. (vi) Most of the metal NC probes used in colorimetric assays are related to a single metal core (Ag, Au, Cu, and Pt), while more sensitivity and accuracy may be achieved by the designed bimetallic cores. In conclusion, the broadly developed FMNCs are dependent on the capping agent species and synthesis conditions reported so far, while a few of them have been used for colorimetric assays as well as the absence of colorimetric detections regarding other important ions and biomarkers (e.g., Se^{2-}, SCN^{-}, Fe^{3+}, UO_2^{2+}, VEGF 165, HER2, and BCR/ABL fusion gene). Colorimetric tests based on FMNCs should be further developed for diagnostic purposes. This will enable them to be employed in a broader range of conditions in the years to come.

AUTHOR INFORMATION

Corresponding Authors

Amirhosein Kefayat − *Biomaterials and Tissue Engineering Research Group, Department of Interdisciplinary Technologies, Breast Cancer Research Center, Motamed Cancer Institute, ACECR, Tehran, Iran; Department of Oncology, Isfahan University of Medical Sciences, Isfahan, Iran;* orcid.org/0000-0002-0616-8870; Email: ahkefayat@yahoo.com

Fatemeh Molaabasi − *Biomaterials and Tissue Engineering Research Group, Department of Interdisciplinary Technologies, Breast Cancer Research Center, Motamed Cancer Institute, ACECR, Tehran, Iran;* orcid.org/0000-0002-9242-9319; Email: molaabasi.fatemeh@yahoo.com

Authors

Nasim Mohseni − *Biomaterials and Tissue Engineering Research Group, Department of Interdisciplinary Technologies, Breast Cancer Research Center, Motamed Cancer Institute, ACECR, Tehran, Iran*

Mohammad Moodi − *Department of Materials Science and Engineering, Ferdowsi University of Mashhad, Mashhad, Iran*

Farhad Shokati − *Biomaterials and Tissue Engineering Research Group, Department of Interdisciplinary Technologies, Breast Cancer Research Center, Motamed Cancer Institute, ACECR, Tehran, Iran*

Complete contact information is available at: https://pubs.acs.org/10.1021/acsomega.3c06884

Author Contributions

Nasim Mohseni created the graphical abstract and wrote the initial draft and the final manuscript. Mohammad Moodi edited the figures and manuscript as per journal guidelines. Farhad Shokati performed the preliminary data analysis. Amirhossein Kefayat and Fatemeh Molaabasi created the figures, supervised the project, and amended and evaluated the final draft.

Notes

The authors declare no competing financial interest.

ABBREVIATIONS USED

AA, ascorbic acid; ABTS, 2,2′-azino-bis(3-ethylbenzothiazoline-6-sulfonic acid; AgNCs, silver nanoclusters; AgNPs, silver nanoparticles; ALP, alkaline phosphatase; ATP, adenosine triphosphate; AuNCs, gold nanoclusters; AuNCs-LPs, AuNCs-loaded liposomes; AuNPs, gold nanoparticles; AIE, aggregation-induced emission; AIEE, aggregation-induced emission enhancement; BGP, bitter gourd polysaccharide; BSA, bovine serum albumin; CD, circular dichroism; CDs, carbon dots; CS, chitosan; CTAB, cetyltrimethylammonium bromide; Cys, cysteine; DA, dopamine; DAP, 2,3-diamino phenazine; DC, doxycycline; 3D GF, three-dimensional graphene foam; GO, graphene oxide; DLW, direct laser writing; DNP, 2,4-dinitrophenol; ELISAs, enzyme-linked immunosorbent assays; FA, folic acid; FMNCs, fluorescent metal nanoclusters; GLP, ganoderma lucidum polysaccharide; GMP, guanosine monophosphate; GR, glutathione reductase; GSH, glutathione; GSSG, glutathione oxidized; Hb, hemoglobin; HER2, human epidermal growth factor receptor-2; HPLC, high-performance liquid chromatography; HQ, hydroquinone; HRP, horseradish peroxidase; IC, ion chromatography; ICP-AES, inductively coupled plasma atomic emission spectrometry; ICPMS, inductively coupled plasma mass spectroscopy; LNT, lentinan; LOD, limit of detection; OA, oriented attachment; OPD, *o*-phenylenediamine; OR, Ostwald ripening; MA, methamphetamine; MCA, 1-methyl-2-imidazolecarboxaldehyde; miRNAs, microRNAs; MMPs, matrix metalloproteinases; MPA, mercaptopropionic acid; MSA, mercaptosuccinic acid; MUA, mercaptoundecanoic acid; PA, penicillamine; PCR, polymerase chain reaction; PEI, polyethylenimine; PPi, pyrophosphate; PtNCs, platinum nanoclusters; QDs, quantum dots; RGO, reduced graphene oxide; MB, methylene blue; TBAB, borane *tert*-butylamine; TBHQ, *tert*-butyl hydroquinone; TC, tetracycline; THPC, tetrakis(hydroxymethyl) phosphonium chloride; TMB, 3,3′,5,5′-tetramethylbenzidine; UHT, ultrahigh temperature; S-AIE, self-assembly induced emission; *S. typhimurium*, *Salmonella typhimurium*; *S. aureus*, *Staphylococcus aureus*; ZIF, zeolitic imidazolate frameworks

REFERENCES

(1) Su, S.; Li, J.; Yao, Y.; Sun, Q.; Zhao, Q.; Wang, F.; Li, Q.; Liu, X.; Wang, L. Colorimetric Analysis of Carcinoembryonic Antigen Using Highly Catalytic Gold Nanoparticles-Decorated MoS2 Nanocomposites. *ACS Appl. Bio Mater.* **2019**, *2* (1), 292−298.

(2) Sun, J.; Jin, Y. Fluorescent Au Nanoclusters: Recent Progress and Sensing Applications. *J. Mater. Chem. C* **2014**, *2* (38), 8000−8011.

(3) Ma, F.; Yuan, C. W.; Liu, J. N.; Cao, J. H.; Wu, D. Y. Colorimetric Immunosensor Based on Au@g-C3N4-Doped Sponge-like 3D Network Cellulose Hydrogels for Detecting α-Fetoprotein. *ACS Appl. Mater. Interfaces* **2019**, *11* (22), 19902−19912.

(4) Kim, H.; Park, M.; Hwang, J.; Kim, J. H.; Chung, D. R.; Lee, K. S.; Kang, M. Development of Label-Free Colorimetric Assay for

MERS-CoV Using Gold Nanoparticles. *ACS Sens.* **2019**, *4* (5), 1306−1312.
(5) Gao, Y.; Wu, Y.; Huang, P.; Wu, F.-Y. Carbon Dot-Encapsulated Plasmonic Core-Satellite Nanoprobes for Sensitive Detection of Cancer Biomarkers via Dual-Mode Colorimetric and Fluorometric Immunoassay. *ACS Appl. Nano Mater.* **2022**, *5* (8), 11539−11548.
(6) Facure, M. H. M.; Andre, R. S.; Mercante, L. A.; Correa, D. S. Colorimetric Detection of Antioxidants in Food Samples Using MnO2/Graphene Quantum Dot Composites with Oxidase-like Activity. *ACS Appl. Nano Mater.* **2022**, *5* (10), 15211−15219.
(7) Beqa, L.; Singh, A. K.; Khan, S. A.; Senapati, D.; Arumugam, S. R.; Ray, P. C. Gold Nanoparticle-Based Simple Colorimetric and Ultrasensitive Dynamic Light Scattering Assay for the Selective Detection of Pb(II) from Paints, Plastics, and Water Samples. *ACS Appl. Mater. Interfaces* **2011**, *3* (3), 668−673.
(8) Wang, L.; Zheng, J.; Li, Y.; Yang, S.; Liu, C.; Xiao, Y.; Li, J.; Cao, Z.; Yang, R. AgNP-DNA@GQDs Hybrid: New Approach for Sensitive Detection of H2O2 and Glucose via Simultaneous AgNP Etching and DNA Cleavage. *Anal. Chem.* **2014**, *86* (24), 12348−12354.
(9) Idros, N.; Chu, D. Triple-Indicator-Based Multidimensional Colorimetric Sensing Platform for Heavy Metal Ion Detections. *ACS Sens.* **2018**, *3* (9), 1756−1764.
(10) Wang, G.; Jin, L.-Y.; Dong, Y.; Wu, X.; Li, Z. Intrinsic Enzyme Mimicking Activity of Gold Nanoclusters upon Visible Light Triggering and Its Application for Colorimetric Trypsin Detection. *Biosens. Bioelectron.* **2015**, *64*, 523−529.
(11) Zhao, T.; Zhou, T.; Yao, Q.; Hao, C.; Chen, X. Metal Nanoclusters: Applications in Environmental Monitoring and Cancer Therapy. *J. Environ. Sci. Heal. - Part C Environ. Carcinog. Ecotoxicol. Rev.* **2015**, *33* (2), 168−187.
(12) Tao, Y.; Lin, Y.; Huang, Z.; Ren, J.; Qu, X. Incorporating Graphene Oxide and Gold Nanoclusters: A Synergistic Catalyst with Surprisingly High Peroxidase-like Activity over a Broad PH Range and Its Application for Cancer Cell Detection. *Adv. Mater.* **2013**, *25* (18), 2594−2599.
(13) Yaraki, M. T.; Zahed Nasab, S.; Zare, I.; Dahri, M.; Moein Sadeghi, M.; Koohi, M.; Tan, Y. N. Biomimetic Metallic Nanostructures for Biomedical Applications, Catalysis, and Beyond. *Ind. Eng. Chem. Res.* **2022**, *61* (22), 7547−7593.
(14) Hu, Y.; Guo, W.; Wei, H. Protein- and Peptide-Directed Approaches to Fluorescent Metal Nanoclusters. *Isr. J. Chem.* **2015**, *55* (6), 682−697.
(15) Oliveira, E.; Núñez, C.; Santos, H. M.; Fernández-Lodeiro, J.; Fernández-Lodeiro, A.; Capelo, J. L.; Lodeiro, C. Revisiting the Use of Gold and Silver Functionalised Nanoparticles as Colorimetric and Fluorometric Chemosensors for Metal Ions. *Sensors Actuators, B Chem.* **2015**, *212*, 297−328.
(16) Bain, D.; Maity, S.; Patra, A. Opportunities and Challenges in Energy and Electron Transfer of Nanocluster Based Hybrid Materials and Their Sensing Applications. *Phys. Chem. Chem. Phys.* **2019**, *21* (11), 5863−5881.
(17) Zhu, L.; Gharib, M.; Becker, C.; Zeng, Y.; Ziefuß, A. R.; Chen, L.; Alkilany, A. M.; Rehbock, C.; Barcikowski, S.; Parak, W. J.; Chakraborty, I. Synthesis of Fluorescent Silver Nanoclusters: Introducing Bottom-Up and Top-Down Approaches to Nano-chemistry in a Single Laboratory Class. *J. Chem. Educ.* **2020**, *97* (1), 239−243.
(18) Huang, C.-C.; Yang, Z.; Lee, K.-H.; Chang, H.-T. Synthesis of Highly Fluorescent Gold Nanoparticles for Sensing Mercury(II). *Angew. Chemie Int. Ed.* **2007**, *46* (36), 6824−6828.
(19) Chen, P.-C.; Yeh, T.-Y.; Ou, C.-M.; Shih, C.-C.; Chang, H.-T. Synthesis of Aluminum Oxide Supported Fluorescent Gold Nanodots for the Detection of Silver Ions. *Nanoscale* **2013**, *5* (11), 4691−4695.
(20) Lin, C.-A. J.; Yang, T.-Y.; Lee, C.-H.; Huang, S. H.; Sperling, R. A.; Zanella, M.; Li, J. K.; Shen, J.-L.; Wang, H.-H.; Yeh, H.-I.; Parak, W. J.; Chang, W. H. Synthesis, Characterization, and Bioconjugation of Fluorescent Gold Nanoclusters toward Biological Labeling Applications. *ACS Nano* **2009**, *3* (2), 395−401.
(21) Muhammed, M. A. H.; Aldeek, F.; Palui, G.; Trapiella-Alfonso, L.; Mattoussi, H. Growth of In Situ Functionalized Luminescent Silver Nanoclusters by Direct Reduction and Size Focusing. *ACS Nano* **2012**, *6* (10), 8950−8961.
(22) Duan, H.; Nie, S. Etching Colloidal Gold Nanocrystals with Hyperbranched and Multivalent Polymers: A New Route to Fluorescent and Water-Soluble Atomic Clusters. *J. Am. Chem. Soc.* **2007**, *129* (9), 2412−2413.
(23) Yuan, X.; Luo, Z.; Zhang, Q.; Zhang, X.; Zheng, Y.; Lee, J. Y.; Xie, J. Synthesis of Highly Fluorescent Metal (Ag, Au, Pt, and Cu) Nanoclusters by Electrostatically Induced Reversible Phase Transfer. *ACS Nano* **2011**, *5* (11), 8800−8808.
(24) Li, R.; Wang, C.; Bo, F.; Wang, Z.; Shao, H.; Xu, S.; Cui, Y. Microwave-Assisted Synthesis of Fluorescent Ag Nanoclusters in Aqueous Solution. *ChemPhysChem* **2012**, *13* (8), 2097−2101.
(25) Díez, I.; Pusa, M.; Kulmala, S.; Jiang, H.; Walther, A.; Goldmann, A. S.; Müller, A. H. E.; Ikkala, O.; Ras, R. H. A. Color Tunability and Electrochemiluminescence of Silver Nanoclusters. *Angew. Chemie - Int. Ed.* **2009**, *48* (12), 2122−2125.
(26) Wu, Z.; Lanni, E.; Chen, W.; Bier, M. E.; Ly, D.; Jin, R. High Yield, Large Scale Synthesis of Thiolate-Protected Ag7 Clusters. *J. Am. Chem. Soc.* **2009**, *131* (46), 16672−16674.
(27) Xu, H.; Suslick, K. S. Sonochemical Synthesis of Highly Fluorescent Ag Nanoclusters. *ACS Nano* **2010**, *4* (6), 3209−3214.
(28) Zhou, Y.; Yu, Y.; Chai, Y.; Yuan, R. Electrochemical Synthesis of Silver Nanoclusters on Electrochemiluminescent Resonance Energy Transfer Amplification Platform for Apo-A1 Detection. *Talanta* **2018**, *181*, 32−37.
(29) Kunwar, P.; Soman, P. Direct Laser Writing of Fluorescent Silver Nanoclusters: A Review of Methods and Applications. *ACS Appl. Nano Mater.* **2020**, *3* (8), 7325−7342.
(30) Shamsipur, M.; Molaei, K.; Molaabasi, F.; Hosseinkhani, S.; Taherpour, A.; Sarparast, M.; Moosavifard, S. E.; Barati, A. Aptamer-Based Fluorescent Biosensing of Adenosine Triphosphate and Cytochrome c via Aggregation-Induced Emission Enhancement on Novel Label-Free DNA-Capped Silver Nanoclusters/Graphene Oxide Nanohybrids. *ACS Appl. Mater. Interfaces* **2019**, *11*, 46077.
(31) Molaabasi, F.; Sarparast, M.; Shamsipur, M.; Irannejad, L.; Moosavi-Movahedi, A. A.; Ravandi, A.; Hajipour Verdom, B.; Ghazfar, R. Shape-Controlled Synthesis of Luminescent Hemoglobin Capped Hollow Porous Platinum Nanoclusters and Their Application to Catalytic Oxygen Reduction and Cancer Imaging. *Sci. Rep.* **2018**, *8* (1), 1−18.
(32) Kawasaki, H.; Hamaguchi, K.; Osaka, I.; Arakawa, R. Ph-Dependent Synthesis of Pepsin-Mediated Gold Nanoclusters with Blue Green and Red Fluorescent Emission. *Adv. Funct. Mater.* **2011**, *21* (18), 3508−3515.
(33) Shamsipur, M.; Molaabasi, F.; Sarparast, M.; Roshani, E.; Vaezi, Z.; Alipour, M.; Molaei, K.; Naderi-Manesh, H.; Hosseinkhani, S. Photoluminescence Mechanisms of Dual-Emission Fluorescent Silver Nanoclusters Fabricated by Human Hemoglobin Template: From Oxidation- and Aggregation-Induced Emission Enhancement to Targeted Drug Delivery and Cell Imaging. *ACS Sustain. Chem. Eng.* **2018**, *6* (8), 11123−11137.
(34) Chen, L. Y.; Wang, C. W.; Yuan, Z.; Chang, H. T. Fluorescent Gold Nanoclusters: Recent Advances in Sensing and Imaging. *Anal. Chem.* **2015**, *87* (1), 216−229.
(35) Huang, C.-C.; Liao, H.-Y.; Shiang, Y.-C.; Lin, Z.-H.; Yang, Z.; Chang, H.-T. Synthesis of Wavelength-Tunable Luminescent Gold and Gold/Silver Nanodots. *J. Mater. Chem.* **2009**, *19* (6), 755−759.
(36) Shamsipur, M.; Molaabasi, F.; Shanehsaz, M.; Moosavi-Movahedi, A. A. Novel Blue-Emitting Gold Nanoclusters Confined in Human Hemoglobin, and Their Use as Fluorescent Probes for Copper(II) and Histidine. *Microchim. Acta* **2015**, *182* (5−6), 1131−1141.
(37) Shamsipur, M.; Samandari, L.; Farzin, L.; Molaabasi, F.; Mousazadeh, M. H. Dual-Modal Label-Free Genosensor Based on Hemoglobin@gold Nanocluster Stabilized Graphene Nanosheets for

https://doi.org/10.1021/acsomega.3c06884
ACS Omega 2024, 9, 3143−3163

the Electrochemical Detection of BCR/ABL Fusion Gene. *Talanta* **2020**, *217*, No. 121093.
(38) Wen, F.; Dong, Y.; Feng, L.; Wang, S.; Zhang, S.; Zhang, X. Horseradish Peroxidase Functionalized Fluorescent Gold Nanoclusters for Hydrogen Peroxide Sensing. *Anal. Chem.* **2011**, *83* (4), 1193−1196.
(39) Sarparast, M.; Molaabasi, F.; Ghazfar, R.; Ashtiani, M. M.; Qarai, M. B.; Taherpour, A.; Amyab, S. P.; Shamsipur, M. Efficient Ethanol Oxidation by Hemoglobin-Capped Gold Nanoclusters: The Critical Role of Fe in the Heme Group as an Oxophilic Metal Active Site. *Electrochem. commun.* **2019**, *103*, 42−47.
(40) Liu, C. L.; Wu, H. T.; Hsiao, Y. H.; Lai, C. W.; Shih, C. W.; Peng, Y. K.; Tang, K. C.; Chang, H. W.; Chien, Y. C.; Hsiao, J. K.; Cheng, J. T.; Chou, P. T. Insulin-Directed Synthesis of Fluorescent Gold Nanoclusters: Preservation of Insulin Bioactivity and Versatility in Cell Imaging. *Angew. Chemie - Int. Ed.* **2011**, *50* (31), 7056−7060.
(41) Molaabasi, F.; Babaee, E.; Kefayat, A. 10 - Peptide-Protected Metal Nanoclusters. In *Luminescent Metal Nanoclusters*; Thomas, S., Joseph, K., Appukuttan, S., Mathew, M. S., Eds.; Woodhead Publishing, 2022; pp 281−302. DOI: 10.1016/B978-0-323-88657-4.00003-X. Woodhead Publishing Series in Electronic and Optical Materials
(42) Molaabasi, F.; Kefayat, A.; Ghasemzadeh, A.; Amandadi, M.; Shamsipur, M.; Alipour, M.; Moosavifard, S. E.; Besharati, M.; Hosseinkhani, S.; Sarrami-Forooshani, R. Role of the Probe Sequence/Structure in Developing an Ultra-Efficient Label-Free COVID-19 Detection Method Based on Competitive Dual-Emission Ratiometric DNA-Templated Silver Nanoclusters as Single Fluorescent Probes. *Anal. Chem.* **2022**, *94* (51), 17757−17769.
(43) Shamsipur, M.; Molaabasi, F.; Hosseinkhani, S.; Rahmati, F. Detection of Early Stage Apoptotic Cells Based on Label-Free Cytochrome c Assay Using Bioconjugated Metal Nanoclusters as Fluorescent Probes. *Anal. Chem.* **2016**, *88* (4), 2188−2197.
(44) Luo, Z.; Yuan, X.; Yu, Y.; Zhang, Q.; Leong, D. T.; Lee, J. Y.; Xie, J. From Aggregation-Induced Emission of Au(I)−Thiolate Complexes to Ultrabright Au(0)@Au(I)−Thiolate Core−Shell Nanoclusters. *J. Am. Chem. Soc.* **2012**, *134* (40), 16662−16670.
(45) Zheng, K.; Yuan, X.; Kuah, K.; Luo, Z.; Yao, Q.; Zhang, Q.; Xie, J. Boiling Water Synthesis of Ultrastable Thiolated Silver Nanoclusters with Aggregation-Induced Emission. *Chem. Commun.* **2015**, *51* (82), 15165−15168.
(46) Yao, Q.; Yu, Y.; Yuan, X.; Yu, Y.; Xie, J.; Lee, J. Y. Two-Phase Synthesis of Small Thiolate-Protected Au15 and Au18 Nanoclusters. *Small* **2013**, *9* (16), 2696−2701.
(47) Yu, Y.; Chen, X.; Yao, Q.; Yu, Y.; Yan, N.; Xie, J. Scalable and Precise Synthesis of Thiolated Au10−12, Au15, Au18, and Au25 Nanoclusters via PH Controlled CO Reduction. *Chemistry of Materials* **2013**, *25*, 946.
(48) Kang, X.; Wang, S.; Song, Y.; Jin, S.; Sun, G.; Yu, H.; Zhu, M. Bimetallic Au2Cu6 Nanoclusters: Strong Luminescence Induced by the Aggregation of Copper(I) Complexes with Gold(0) Species. *Angew. Chemie - Int. Ed.* **2016**, *55* (11), 3611−3614.
(49) Huang, Y.; Liu, W.; Feng, H.; Ye, Y.; Tang, C.; Ao, H.; Zhao, M.; Chen, G.; Chen, J.; Qian, Z. Luminescent Nanoswitch Based on Organic-Phase Copper Nanoclusters for Sensitive Detection of Trace Amount of Water in Organic Solvents. *Anal. Chem.* **2016**, *88* (14), 7429−7434.
(50) Huang, Y.; Feng, H.; Liu, W.; Zhou, Y.; Tang, C.; Ao, H.; Zhao, M.; Chen, G.; Chen, J.; Qian, Z. Luminescent Aggregated Copper Nanoclusters Nanoswitch Controlled by Hydrophobic Interaction for Real-Time Monitoring of Acid Phosphatase Activity. *Anal. Chem.* **2016**, *88* (23), 11575−11583.
(51) Huang, Y.; Ji, J.; Zhang, J.; Wang, F.; Lei, J. Host−Guest Recognition-Regulated Aggregation-Induced Emission for in Situ Imaging of MUC1 Protein. *Chem. Commun.* **2020**, *56* (2), 313−316.
(52) Zhao, M.; Qian, Z.; Zhong, M.; Chen, Z.; Ao, H.; Feng, H. Fabrication of Stable and Luminescent Copper Nanocluster-Based AIE Particles and Their Application in β-Galactosidase Activity Assay. *ACS Appl. Mater. Interfaces* **2017**, *9* (38), 32887−32895.
(53) Campisi, S.; Schiavoni, M.; Chan-Thaw, C. E.; Villa, A. Untangling the Role of the Capping Agent in Nanocatalysis: Recent Advances and Perspectives. *Catalysts* **2016**, *6* (12), 185.
(54) Wen, R.; Li, H.; Chen, B.; Wang, L. Facile Preparation of Fluorescent Gold Nanocluster via Polysaccharide-Templated Approach and Its Application for Cu2+ Sensing. *Sensors and Actuators B-chemical* **2017**, *248*, 63−70.
(55) Dong, L.; Li, R.; Wang, L.; Lan, X.; Sun, H.; Zhao, Y.; Wang, L. Green Synthesis of Platinum Nanoclusters Using Lentinan for Sensitively Colorimetric Detection of Glucose. *Int. J. Biol. Macromol.* **2021**, *172*, 289.
(56) Lai, X.; Han, Y.; Zhang, J.; Zhang, J.; Lin, W.; Liu, Z.; Wang, L. Peroxidase-Like Platinum Clusters Synthesized by Ganoderma Lucidum Polysaccharide for Sensitively Colorimetric Detection of Dopamine. *Molecules* **2021**, *26* (9), 2738.
(57) Liu, K.; Zhao, Y.; Zhang, L.; He, M.; Lin, W.; Sun, H.; Liu, Z.; Hu, J.; Wang, L. Biocompatible Platinum Nanoclusters Prepared Using Bitter Gourd Polysaccharide for Colorimetric Detection of Ascorbic Acid. *Biomolecules* **2021**, *11* (5), 647.
(58) Cheng, C.; Yang, L.; Zhong, M.; Deng, W.; Tan, Y.; Xie, Q.; Yao, S. Au Nanocluster-Embedded Chitosan Nanocapsules as Labels for the Ultrasensitive Fluorescence Immunoassay of Escherichia Coli O157:H7. *Analyst* **2018**, *143*, 4067−4073.
(59) Dehghani, Z.; Hosseini, M.; Mohammadnejad, J.; Ganjali, M. R. Novel Colorimetric Sensor Based on Peroxidase-like Activity of Chitosan-Stabilized Au/Pt Nanoclusters for Trace Lead. *Anal. Methods* **2019**, *11* (5), 684−690.
(60) Zhang, Q.; Wang, J.; Meng, Z.; Ling, R.; Ren, H.; Qin, W.; Wu, Z.; Shao, N. Glutathione Disulfide as a Reducing, Capping, and Mass-Separating Agent for the Synthesis and Enrichment of Gold Nanoclusters. *Nanomaterials* **2021**, *11* (9), 2258.
(61) Jiang, X.; Zhang, H.; Yang, C.; Xia, J.; Liu, G.; Luo, X. A Novel Electrostatic Drive Strategy to Prepare Glutathione-Capped Gold Nanoclusters Embedded Quaternized Cellulose Membranes Fluorescent Colorimetric Sensor for Pb(II) and Hg(II) Ions Detection. *Sensors Actuators B Chem.* **2022**, *368*, No. 132046.
(62) Liu, X.; Astruc, D. Atomically Precise Copper Nanoclusters and Their Applications. *Coord. Chem. Rev.* **2018**, *359*, 112−126.
(63) Le Guével, X.; Perez Perrino, M.; Fernández, T. D.; Palomares, F.; Torres, M.-J.; Blanca, M.; Rojo, J.; Mayorga, C. Multivalent Glycosylation of Fluorescent Gold Nanoclusters Promotes Increased Human Dendritic Cell Targeting via Multiple Endocytic Pathways. *ACS Appl. Mater. Interfaces* **2015**, *7* (37), 20945−20956.
(64) Zhao, Q.; Chen, S.; Huang, H.; Zhang, L.; Wang, L.; Liu, F.; Chen, J.; Zeng, Y.; Chu, P. K. Colorimetric and Ultra-Sensitive Fluorescence Resonance Energy Transfer Determination of H2O2 and Glucose by Multi-Functional Au Nanoclusters. *Analyst* **2014**, *139* (6), 1498−1503.
(65) Liao, H.; Liu, G.; Liu, Y.; Li, R.; Fu, W.; Hu, L. Aggregation-Induced Accelerating Peroxidase-like Activity of Gold Nanoclusters and Their Applications for Colorimetric Pb2+ Detection. *Chem. Commun.* **2017**, *53* (73), 10160−10163.
(66) Javed, R.; Zia, M.; Naz, S.; Aisida, S. O.; Ain, N. ul; Ao, Q. Role of Capping Agents in the Application of Nanoparticles in Biomedicine and Environmental Remediation: Recent Trends and Future Prospects. *J. Nanobiotechnology* **2020**, *18* (1), 1−15.
(67) Shankar, S.; Gowthaman, N. S. K.; Arul, P.; Chen, F.; Lim, H. N.; Qin, F.-X. Ultra-Sensitive and Selective Determination of a Phenolic Food Additive Using Protein Capped Gold Nanoclusters: A Dual in-Line Fluorometric and Colorimetric Sensing Probe. *New J. Chem.* **2021**, *45*, 1278−1285.
(68) Ma, S.; Wang, J.; Yang, G.; Yang, J.; Ding, D.; Zhang, M. Copper(II) Ions Enhance the Peroxidase-like Activity and Stability of Keratin-Capped Gold Nanoclusters for the Colorimetric Detection of Glucose. *Microchim. Acta* **2019**, *186*, 1−7.
(69) Xie, R.; Zhang, N.; Qu, Y.; Tang, M.; Zhang, F.; Chai, F.; Su, Z. The Synthesis of Cu Nanoclusters and Their Dual Mode Colorimetric and Fluorescent Sensing for 2,4-Dinitrophenol. *Nanotechnology* **2021**, *33* (2), 25501.

https://doi.org/10.1021/acsomega.3c06884
ACS Omega 2024, 9, 3143−3163

(70) Fu, M.; Li, L.; Yang, D.; Tu, Y.; Yan, J. Colorimetric Detections of Iodide and Mercuric Ions Based on a Regulation of an Enzyme-Like Activity from Gold Nanoclusters. *Spectrochim. Acta Part A Mol. Biomol. Spectrosc.* **2022**, *279*, No. 121450.
(71) Chen, Y.; Phipps, M. L.; Werner, J. H.; Chakraborty, S.; Martinez, J. S. DNA Templated Metal Nanoclusters: From Emergent Properties to Unique Applications. *Acc. Chem. Res.* **2018**, *51* (11), 2756−2763.
(72) Bagheri pebdeni, A.; Hosseini, M. Fast and Selective Whole Cell Detection of Staphylococcus Aureus Bacteria in Food Samples by Paper Based Colorimetric Nanobiosensor Using Peroxidase-like Catalytic Activity of DNA-Au/Pt Bimetallic Nanoclusters. *Microchem. J.* **2020**, *159*, No. 105475.
(73) Du, Z.; Wei, C. Using G-Rich Sequence to Enhance the Peroxidase-Mimicking Activity of DNA-Cu/Ag Nanoclusters for Rapid Colorimetric Detection of Hydrogen Peroxide and Glucose. *ChemistrySelect* **2020**, *5* (17), 5166−5171.
(74) Wu, L.; Wang, L.-Y.; Xie, Z.-J.; Xue, F.; Peng, C. Colorimetric Detection of Hg2+ Based on Inhibiting the Peroxidase-like Activity of DNA−Ag/Pt Nanoclusters. *RSC Adv.* **2016**, *6*, 75384−75389.
(75) Sen, A.; Sester, C.; Poulsen, H.; Hodgkiss, J. M. Accounting for Interaction Kinetics between Gold Nanoparticles and Aptamers Enables High-Performance Colorimetric Sensors. *ACS Appl. Mater. Interfaces* **2022**, *14* (29), 32813−32822.
(76) Song, Y.; Wang, L.; Zhao, J.; Li, H.; Yang, X.; Fu, S.; Qin, X.; Chen, Q.; Jiang, Y.; Man, C. A Novel Colorimetric Sensor Using Aptamers to Enhance Peroxidase-like Property of Gold Nanoclusters for Detection of Escherichia Coli O157:H7 in Milk. *Int. Dairy J.* **2022**, *128*, No. 105318.
(77) Chen, Q.; Gao, R.; Jia, L. Enhancement of the Peroxidase-like Activity of Aptamers Modified Gold Nanoclusters by Bacteria for Colorimetric Detection of Salmonella Typhimurium. *Talanta* **2021**, *221*, No. 121476.
(78) Ma, Y.; Shen, X.-F.; Liu, F.; Pang, Y.-H. Colorimetric Detection toward Halide Ions by a Silver Nanocluster Hydrogel. *Talanta* **2020**, *211*, No. 120717.
(79) Liu, Q. Determination of Mercury and Methylmercury in Seafood by Ion Chromatography Using Photo-Induced Chemical Vapor Generation Atomic Fluorescence Spectrometric Detection. *Microchem. J.* **2010**, *95* (2), 255−258.
(80) Gupta, V. K.; Ganjali, M. R.; Norouzi, P.; Khani, H.; Nayak, A.; Agarwal, S. Electrochemical Analysis of Some Toxic Metals by Ion−Selective Electrodes. *Crit. Rev. Anal. Chem.* **2011**, *41* (4), 282−313.
(81) Ghaedi, M.; Reza Fathi, M.; Shokrollahi, A.; Shajarat, F. Highly Selective and Sensitive Preconcentration of Mercury Ion and Determination by Cold Vapor Atomic Absorption Spectroscopy. *Anal. Lett.* **2006**, *39* (6), 1171−1185.
(82) Syty, A.; Christensen, R. G.; Rains, T. C. Determination of Added Chromium(III) and Chromium(VI) in Natural Water by Ion-Pairing High-Performance Liquid Chromatography with Detection by Atomic Absorption Spectrometry. *J. Anal. At. Spectrom.* **1988**, *3* (1), 193−197.
(83) Djedjibegovic, J.; Larssen, T.; Skrbo, A.; Marjanović, A.; Sober, M. Contents of Cadmium, Copper, Mercury and Lead in Fish from the Neretva River (Bosnia and Herzegovina) Determined by Inductively Coupled Plasma Mass Spectrometry (ICP-MS). *Food Chem.* **2012**, *131* (2), 469−476.
(84) Shoaee, H.; Roshdi, M.; Khanlarzadeh, N.; Beiraghi, A. Simultaneous Preconcentration of Copper and Mercury in Water Samples by Cloud Point Extraction and Their Determination by Inductively Coupled Plasma Atomic Emission Spectrometry. *Spectrochim. Acta Part A Mol. Biomol. Spectrosc.* **2012**, *98*, 70−75.
(85) Chen, N.; Zhang, Y.; Liu, H.; Wu, X.; Li, Y.; Miao, L.; Shen, Z.; Wu, A. High-Performance Colorimetric Detection of Hg2+ Based on Triangular Silver Nanoprisms. *ACS Sens.* **2016**, *1* (5), 521−527.
(86) Qu, F.; Li, N. B.; Luo, H. Q. Polyethyleneimine-Templated Ag Nanoclusters: A New Fluorescent and Colorimetric Platform for Sensitive and Selective Sensing Halide Ions and High Disturbance-Tolerant Recognitions of Iodide and Bromide in Coexistence with Chloride under Condition of High. *Anal. Chem.* **2012**, *84* (23), 10373−10379.
(87) Tao, Y.; Lin, Y.; Huang, Z.; Ren, J.; Qu, X. Poly(Acrylic Acid)-Templated Silver Nanoclusters as a Platform for Dual Fluorometric Turn-on and Colorimetric Detection of Mercury (II) Ions. *Talanta* **2012**, *88*, 290−294.
(88) Yu, L.; Zhang, L.; Ren, G.; Li, S.; Zhu, B.; Chai, F.; Qu, F.; Wang, C.; Su, Z. Multicolorful Fluorescent-Nanoprobe Composed of Au Nanocluster and Carbon Dots for Colorimetric and Fluorescent Sensing Hg2+ and Cr6+. *Sensors Actuators, B Chem.* **2018**, *262*, 678−686.
(89) Guo, Y.; Amunyela, H. T. N. N.; Cheng, Y.; Xie, Y.; Yu, H.; Yao, W.; Li, H. W.; Qian, H. Natural Protein-Templated Fluorescent Gold Nanoclusters: Syntheses and Applications. *Food Chem.* **2021**, *335*, No. 127657.
(90) Wang, Y.-W.; Tang, S.; Yang, H.-H.; Song, H. A Novel Colorimetric Assay for Rapid Detection of Cysteine and Hg2+ Based on Gold Clusters. *Talanta* **2016**, *146*, 71−74.
(91) Huang, Y.-Q.; Fu, S.; Wang, Y.-S.; Xue, J.; Xiao, X.; Chen, S.-H.; Zhou, B. Protamine-Gold Nanoclusters as Peroxidase Mimics and the Selective Enhancement of Their Activity by Mercury Ions for Highly Sensitive Colorimetric Assay of Hg(II). *Anal. Bioanal. Chem.* **2018**, *410*, 7385−7394.
(92) Wang, H.-B.; Bai, H.; Wang, Y.-S.; Gan, T.; Liu, Y. Highly Selective Fluorimetric and Colorimetric Sensing of Mercury(II) by Exploiting the Self-Assembly-Induced Emission of 4-Chlorothiophenol Capped Copper Nanoclusters. *Microchim. Acta* **2020**, *187*, 1−9.
(93) Zheng, S.; Gu, H.; Yin, D.; Zhang, J.; Li, W.; Fu, Y. Biogenic Synthesis of AuPd Nanocluster as a Peroxidase Mimic and Its Application for Colorimetric Assay of Acid Phosphatase. *Colloids Surfaces A Physicochem. Eng. Asp.* **2020**, *589*, No. 124444.
(94) Cai, Y.; Wang, J.; Niu, L.; Zhang, Y.; Liu, X.; Liu, C.; Yang, S.; Qi, H.; Liu, A. Selective Colorimetric Sensing of Sub-Nanomolar Hg2+ Based on Its Significantly Enhancing Peroxidase Mimics of Silver/Copper Nanoclusters. *Analyst* **2021**, *146* (14), 4630−4635.
(95) Liu, R.; Zuo, L.; Huang, X.; Liu, S.; Yang, G.; Li, S.; Lv, C. Colorimetric Determination of Lead(II) or Mercury(II) Based on Target Induced Switching of the Enzyme-like Activity of Metallothionein-Stabilized Copper Nanoclusters. *Microchim. Acta* **2019**, *186*, 1−8.
(96) Xue, Q.; Li, X.; Peng, Y.; Liu, P.; Peng, H.; Niu, X. Polyethylenimine-Stabilized Silver Nanoclusters Act as an Oxidoreductase Mimic for Colorimetric Determination of Chromium(VI). *Microchim. Acta* **2020**, DOI: 10.1007/s00604-020-04232-8.
(97) Chaiendoo, K.; Tuntulani, T.; Ngeontae, W. A Highly Selective Colorimetric Sensor for Ferrous Ion Based on Polymethylacrylic Acid-Templated Silver Nanoclusters. *Sensors Actuators, B Chem.* **2015**, *207*, 658−667.
(98) Liu, L.; Du, J.; Liu, W. e.; Guo, Y.; Wu, G.; Qi, W.; Lu, X. Enhanced His@AuNCs Oxidase-like Activity by Reduced Graphene Oxide and Its Application for Colorimetric and Electrochemical Detection of Nitrite. *Anal. Bioanal. Chem.* **2019**, *411* (10), 2189−2200.
(99) Shojaeifard, Z.; Hemmateenejad, B.; Shamsipur, M.; Ahmadi, R. Dual Fluorometric and Colorimetric Sensor Based on Quenching Effect of Copper (II) Sulfate on the Copper Nanocluster for Determination of Sulfide Ion in Water Samples. *J. Photochem. Photobiol. A Chem.* **2019**, *384*, 112030.
(100) Liao, H.; Hu, L.; Zhang, Y.; Yu, X.; Liu, Y.; Li, R. A Highly Selective Colorimetric Sulfide Assay Based on the Inhibition of the Peroxidase-like Activity of Copper Nanoclusters. *Microchim. Acta* **2018**, *185*, 1−6.
(101) Kuo, H.-C.; Ye, Z.-T.; Tseng, S. F.; Tsou, S. X.; Huang, S. W.; Tsai, C.-W. Noninvasive Direct Bilirubin Detection by Spectral Analysis of Color Images Using a Mini-LED Light Source. *Discovery Nano* **2023**, *18* (1), 16.
(102) Aparna, R. S.; Anjali, A. D.; John, N.; Abha, K.; Syamchand, S. S.; George, S. Blue Emitting Copper Nanoclusters as Colorimetric

https://doi.org/10.1021/acsomega.3c06884
ACS Omega 2024, 9, 3143−3163

and Fluorescent Probe for the Selective Detection of Bilirubin. *Spectrochim. Acta - Part A Mol. Biomol. Spectrosc.* **2018**, *199*, 123−129.
(103) Qu, F.; Chen, P.; Zhu, S.; You, J. High Selectivity of Colorimetric Detection of P-Nitrophenol Based on Ag Nanoclusters. *Spectrochim. Acta Part A Mol. Biomol. Spectrosc.* **2017**, *171*, 449−453.
(104) Du, Y.; Fang, J.; Wang, H.; Yang, Y. Inducible Sequential Oxidation Process in Water-Soluble Copper Nanoclusters for Direct Colorimetric Assay of Hydrogen Peroxide in a Wide Dynamic and Sampling Range. *ACS Appl. Mater. Interfaces* **2017**, *9* (12), 11035−11044.
(105) Yan, Z.; Niu, Q.; Mou, M.; Wu, Y.; Liu, X.; Liao, S. A Novel Colorimetric Method Based on Copper Nanoclusters with Intrinsic Peroxidase-like for Detecting Xanthine in Serum Samples. *J. Nanoparticle Res.* **2017**, *19*, 1−12.
(106) Shi, Y.; Wang, J.; Mu, K.; Liu, S.; Yang, G.; Zhang, M.; Yang, J. Copper (II) Ion-Modified Gold Nanoclusters as Peroxidase Mimetics for the Colorimetric Detection of Pyrophosphate. *Sensors* **2021**, *21* (16), 5538.
(107) Yang, X.-H.; Ling, J.; Peng, J.; Cao, Q.-E.; Wang, L.; Ding, Z.-T.; Xiong, J. Catalytic Formation of Silver Nanoparticles by Bovine Serum Albumin Protected-Silver Nanoclusters and Its Application for Colorimetric Detection of Ascorbic Acid. *Spectrochim. Acta Part A Mol. Biomol. Spectrosc.* **2013**, *106*, 224−230.
(108) Qiu, N.; Liu, Y.; Guo, R. Electrodeposition-Assisted Rapid Preparation of Pt Nanocluster/3D Graphene Hybrid Nanozymes with Outstanding Multiple Oxidase-Like Activity for Distinguishing Colorimetric Determination of Dihydroxybenzene Isomers. *ACS Appl. Mater. Interfaces* **2020**, *12* (13), 15553−15561.
(109) Jiang, S.; Zhang, Y.; Yang, Y.; Huang, Y.; Ma, G.; Luo, Y.; Huang, P.; Lin, J. Glucose Oxidase-Instructed Fluorescence Amplification Strategy for Intracellular Glucose Detection. *ACS Appl. Mater. Interfaces* **2019**, *11* (11), 10554−10558.
(110) Wen, J.; Li, N.; Li, D.; Zhang, M.; Lin, Y.; Liu, Z.; Lin, X.; Shui, L. Cesium-Doped Graphene Quantum Dots as Ratiometric Fluorescence Sensors for Blood Glucose Detection. *ACS Appl. Nano Mater.* **2021**, *4* (8), 8437−8446.
(111) Hu, Y.; Cheng, H.; Zhao, X.; Wu, J.; Muhammad, F.; Lin, S.; He, J.; Zhou, L.; Zhang, C.; Deng, Y.; Wang, P.; Zhou, Z.; Nie, S.; Wei, H. Surface-Enhanced Raman Scattering Active Gold Nanoparticles with Enzyme-Mimicking Activities for Measuring Glucose and Lactate in Living Tissues. *ACS Nano* **2017**, *11* (6), 5558−5566.
(112) Liu, L.; Ma, Q.; Li, Y.; Liu, Z.; Su, X. A Novel Signal-off Electrochemiluminescence Biosensor for the Determination of Glucose Based on Double Nanoparticles. *Biosens. Bioelectron.* **2015**, *63*, 519−524.
(113) Yuan, J.; Cen, Y.; Kong, X.-J.; Wu, S.; Liu, C.-L.; Yu, R.-Q.; Chu, X. MnO2-Nanosheet-Modified Upconversion Nanosystem for Sensitive Turn-On Fluorescence Detection of H2O2 and Glucose in Blood. *ACS Appl. Mater. Interfaces* **2015**, *7* (19), 10548−10555.
(114) Yu, D.; Wang, P.; Zhao, Y.; Fan, A. Iodophenol Blue-Enhanced Luminol Chemiluminescence and Its Application to Hydrogen Peroxide and Glucose Detection. *Talanta* **2016**, *146*, 655−661.
(115) Chang, Q.; Tang, H. Optical Determination of Glucose and Hydrogen Peroxide Using a Nanocomposite Prepared from Glucose Oxidase and Magnetite Nanoparticles Immobilized on Graphene Oxide. *Microchim. Acta* **2014**, *181* (5−6), 527−534.
(116) Chi, J.; Guo, M.; Zhang, C.; Zhang, Y.; Ai, S.; Hou, J.; Wu, P.; Li, X. Glucose Oxidase and Au Nanocluster Co-Encapsulated Metal-Organic Frameworks as a Sensitive Colorimetric Sensor for Glucose Based on a Cascade Reaction. *New J. Chem.* **2020**, *44* (31), 13344−13349.
(117) Sun, F.; Liang, Y.; Jin, L.; Shi, J.; Shang, L. Weak Interaction-Tailored Catalytic Interface of Ultrasmall Gold Nanoclusters as Enzyme Mimics for Enhanced Colorimetric Biosensing. *ACS Appl. Mater. Interfaces* **2021**, *13* (48), 58209−58219.
(118) Feng, J.; Huang, P.; Wu, F. Gold-Platinum Bimetallic Nanoclusters with Enhanced Peroxidase-like Activity and Their Integrated Agarose Hydrogel-Based Sensing Platform for the Colorimetric Analysis of Glucose Levels in Serum. *Analyst* **2017**, *142*, 4106−4115.
(119) Sun, H.; Zhang, J.; Wang, M.; Su, X. Ratiometric Fluorometric and Colorimetric Dual-Mode Sensing of Glucose Based on Gold-Platinum Bimetallic Nanoclusters. *Microchem. J.* **2022**, *179*, No. 107574.
(120) Jin, L.; Meng, Z.; Zhang, Y.; Cai, S.; Zhang, Z.; Li, C.; Shang, L.; Shen, Y. Ultrasmall Pt Nanoclusters as Robust Peroxidase Mimics for Colorimetric Detection of Glucose in Human Serum. *ACS Appl. Mater. Interfaces* **2017**, *9* (11), 10027−10033.
(121) Hu, L.; Liao, H.; Feng, L.; Wang, M.; Fu, W. Accelerating the Peroxidase-Like Activity of Gold Nanoclusters at Neutral PH for Colorimetric Detection of Heparin and Heparinase Activity. *Anal. Chem.* **2018**, *90* (10), 6247−6252.
(122) Sun, H.; Wang, N.; Zhang, L.; Meng, H.; Li, Z. Aptamer-Based Sensors for Thrombin Detection Application. *Chemosensors* **2022**, *10* (7), 255.
(123) Zheng, C.; Zheng, A.-X.; Liu, B.; Zhang, X.-L.; He, Y.; Li, J.; Yang, H.-H.; Chen, G. One-Pot Synthesized DNA-Templated Ag/Pt Bimetallic Nanoclusters as Peroxidase Mimics for Colorimetric Detection of Thrombin. *Chem. Commun.* **2014**, *50* (86), 13103−13106.
(124) Dehghani, Z.; Mohammadnejad, J.; Hosseini, M. A New Colorimetric Assay for Amylase Based on Starch-Supported Cu/Au Nanocluster Peroxidase-like Activity. *Anal. Bioanal. Chem.* **2019**, *411*, 3621−3629.
(125) Kaur, J.; Singh, P. K. Trypsin Detection Strategies: A Review. *Crit. Rev. Anal. Chem.* **2022**, *52* (5), 949−967.
(126) Dadmehr, M.; Mortezaei, M.; Korouzhdehi, B. Dual Mode Fluorometric and Colorimetric Detection of Matrix Metalloproteinase MMP-9 as a Cancer Biomarker Based on AuNPs@gelatin/AuNCs Nanocomposite. *Biosens. Bioelectron.* **2023**, *220*, No. 114889.
(127) Wang, J. H.; Wang, K.; Bartling, B.; Liu, C.-C. The Detection of Alkaline Phosphatase Using an Electrochemical Biosensor in a Single-Step Approach. *Sensors* **2009**, *9* (11), 8709−8721.
(128) Dong, L.; Miao, Q.; Hai, Z.; Yuan, Y.; Liang, G. Enzymatic Hydrogelation-Induced Fluorescence Turn-Off for Sensing Alkaline Phosphatase in Vitro and in Living Cells. *Anal. Chem.* **2015**, *87* (13), 6475−6478.
(129) Gao, Z.; Deng, K.; Wang, X. D.; Miró, M.; Tang, D. High-Resolution Colorimetric Assay for Rapid Visual Readout of Phosphatase Activity Based on Gold/Silver Core/Shell Nanorod. *ACS Appl. Mater. Interfaces* **2014**, *6* (20), 18243−18250.
(130) Ni, P.; Chen, C.; Jiang, Y.; Zhang, C.; Wang, B.; Cao, B.; Li, C.; Lu, Y. Gold Nanoclusters-Based Dual-Channel Assay for Colorimetric and Turn-on Fluorescent Sensing of Alkaline Phosphatase. *Sensors Actuators, B Chem.* **2019**, *301*, No. 127080.
(131) Qu, F.; Li, N. B.; Luo, H. Q. Highly Sensitive Fluorescent and Colorimetric PH Sensor Based on Polyethylenimine-Capped Silver Nanoclusters. *Langmuir* **2013**, *29* (4), 1199−1205.
(132) Kuśmierek, K.; Chwatko, G.; Głowacki, R.; Bald, E. Determination of Endogenous Thiols and Thiol Drugs in Urine by HPLC with Ultraviolet Detection. *J. Chromatogr. B Anal. Technol. Biomed. Life Sci.* **2009**, *877* (28), 3300−3308.
(133) Toyo'oka, T. Recent Advances in Separation and Detection Methods for Thiol Compounds in Biological Samples. *J. Chromatogr. B Anal. Technol. Biomed. Life Sci.* **2009**, *877* (28), 3318−3330.
(134) Lee, J. S.; Ulmann, P. A.; Han, M. S.; Mirkin, C. A. A DNA - Gold Nanoparticle-Based Colorimetric Competition Assay for the Detection of Cysteine. *Nano Lett.* **2008**, *8* (2), 529−533.
(135) Niu, L. Y.; Guan, Y. S.; Chen, Y. Z.; Wu, L. Z.; Tung, C. H.; Yang, Q. Z. BODIPY-Based Ratiometric Fluorescent Sensor for Highly Selective Detection of Glutathione over Cysteine and Homocysteine. *J. Am. Chem. Soc.* **2012**, *134* (46), 18928−18931.
(136) Yin, J.; Kwon, Y.; Kim, D.; Lee, D.; Kim, G.; Hu, Y.; Ryu, J. H.; Yoon, J. Cyanine-Based Fluorescent Probe for Highly Selective Detection of Glutathione in Cell Cultures and Live Mouse Tissues. *J. Am. Chem. Soc.* **2014**, *136* (14), 5351−5358.

https://doi.org/10.1021/acsomega.3c06884
ACS Omega 2024, 9, 3143−3163

(137) Wang, W.; Li, L.; Liu, S.; Ma, C.; Zhang, S. Determination of Physiological Thiols by Electrochemical Detection with Piazselenole and Its Application in Rat Breast Cancer Cells 4T-1. *J. Am. Chem. Soc.* **2008**, *130* (33), 10846−10847.
(138) Wang, W.; Rusin, O.; Xu, X.; Kim, K. K.; Escobedo, J. O.; Fakayode, S. O.; Fletcher, K. A.; Lowry, M.; Schowalter, C. M.; Lawrence, C. M.; Fronczek, F. R.; Warner, I. M.; Strongin, R. M. Detection of Homocysteine and Cysteine. *J. Am. Chem. Soc.* **2005**, *127* (45), 15949−15958.
(139) Yuan, X.; Tay, Y.; Dou, X.; Luo, Z.; Leong, D. T.; Xie, J. Glutathione-Protected Silver Nanoclusters as Cysteine-Selective Fluorometric and Colorimetric Probe. *Anal. Chem.* **2013**, *85* (3), 1913−1919.
(140) Li, J.-J.; Qiao, D.; Yang, S.-Z.; Weng, G.; Zhu, J.; Zhao, J. Colorimetric Determination of Cysteine Based on Inhibition of GSH-Au/Pt NCs as Peroxidase Mimic. *Spectrochim. Acta. A. Mol. Biomol. Spectrosc.* **2021**, *248*, No. 119257.
(141) Sudeep, P. K.; Joseph, S. T. S.; Thomas, K. G. Selective Detection of Cysteine and Glutathione Using Gold Nanorods. *J. Am. Chem. Soc.* **2005**, *127* (18), 6516−6517.
(142) Hosseini, M.; Ahmadi, E.; Borghei, Y.-S.; Reza Ganjali, M. A New Fluorescence Turn-on Nanobiosensor for the Detection of Micro-RNA-21 Based on a DNA−Gold Nanocluster. *Methods Appl. Fluoresc.* **2017**, *5* (1), No. 015005.
(143) Feng, J.; Huang, P.; Shi, S.; Deng, K. Y.; Wu, F. Y. Colorimetric Detection of Glutathione in Cells Based on Peroxidase-like Activity of Gold Nanoclusters: A Promising Powerful Tool for Identifying Cancer Cells. *Anal. Chim. Acta* **2017**, *967*, 64−69.
(144) Liu, C.; Cai, Y.; Wang, J.; Liu, X.; Ren, H.; Yan, L.; Zhang, Y.; Yang, S.; Guo, J.; Liu, A. Facile Preparation of Homogeneous Copper Nanoclusters Exhibiting Excellent Tetraenzyme Mimetic Activities for Colorimetric Glutathione Sensing and Fluorimetric Ascorbic Acid Sensing. *ACS Appl. Mater. Interfaces* **2020**, *12* (38), 42521−42530.
(145) Jiang, C.; Zhang, C.; Song, J.; Ji, X.; Wang, W. Cytidine-Gold Nanoclusters as Peroxidase Mimetic for Colorimetric Detection of Glutathione (GSH), Glutathione Disulfide (GSSG) and Glutathione Reductase (GR). *Spectrochim. Acta Part A Mol. Biomol. Spectrosc.* **2021**, *250*, No. 119316.
(146) Song, Y.; Qiao, J.; Liu, W.; Qi, L. Colorimetric Detection of Serum Doxycycline with D-Histidine-Functionalized Gold Nanoclusters as Nanozymes. *Analyst* **2020**, *145* (10), 3564−3568.
(147) Zhang, Z.; Tian, Y.; Huang, P.; Wu, F. Using Target-Specific Aptamers to Enhance the Peroxidase-like Activity of Gold Nanoclusters for Colorimetric Detection of Tetracycline Antibiotics. *Talanta* **2020**, *208*, No. 120342.
(148) Zhao, Q.; Huang, H.; Zhang, L.; Wang, L.; Zeng, Y.; Xia, X.; Liu, F.; Chen, Y. Strategy to Fabricate Naked-Eye Readout Ultrasensitive Plasmonic Nanosensor Based on Enzyme Mimetic Gold Nanoclusters. *Anal. Chem.* **2016**, *88* (2), 1412−1418.
(149) Woo, S. M.; Gabardo, C. M.; Soleymani, L. Prototyping of Wrinkled Nano-/Microstructured Electrodes for Electrochemical DNA Detection. *Anal. Chem.* **2014**, *86* (24), 12341−12347.
(150) Nano, A.; Furst, A. L.; Hill, M. G.; Barton, J. K. DNA Electrochemistry: Charge-Transport Pathways through DNA Films on Gold. *J. Am. Chem. Soc.* **2021**, *143* (30), 11631−11640.
(151) Embrechts, J.; Lemière, F.; Van Dongen, W.; Esmans, E. L.; Buytaert, P.; Van Marck, E.; Kockx, M.; Makar, A. Detection of Estrogen DNA-Adducts in Human Breast Tumor Tissue and Healthy Tissue by Combined Nano LC-Nano ES Tandem Mass Spectrometry. *J. Am. Soc. Mass Spectrom.* **2003**, *14* (5), 482−491.
(152) Aman, R.; Mahas, A.; Mahfouz, M. Nucleic Acid Detection Using CRISPR/Cas Biosensing Technologies. *ACS Synth. Biol.* **2020**, *9* (6), 1226−1233.
(153) Franzini, R. M.; Kool, E. T. Organometallic Activation of a Fluorogen for Templated Nucleic Acid Detection. *Org. Lett.* **2008**, *10* (14), 2935−2938.
(154) Bronder, T. S.; Jessing, M. P.; Poghossian, A.; Keusgen, M.; Schöning, M. J. Detection of PCR-Amplified Tuberculosis DNA Fragments with Polyelectrolyte-Modified Field-Effect Sensors. *Anal. Chem.* **2018**, *90* (12), 7747−7753.
(155) Torrente-Rodríguez, R. M.; Ruiz-Valdepeñas Montiel, V.; Campuzano, S.; Farchado-Dinia, M.; Barderas, R.; San Segundo-Acosta, P.; Montoya, J. J.; Pingarron, J. M. Fast Electrochemical MiRNAs Determination in Cancer Cells and Tumor Tissues with Antibody-Functionalized Magnetic Microcarriers. *ACS Sens.* **2016**, *1* (7), 896−903.
(156) Fakhri, N.; Abarghoei, S.; Dadmehr, M.; Hosseini, M.; Sabahi, H.; Ganjali, M. R. Paper Based Colorimetric Detection of MiRNA-21 Using Ag/Pt Nanoclusters. *Spectrochim. Acta. A. Mol. Biomol. Spectrosc.* **2020**, *227*, No. 117529.
(157) Borghei, Y.-S.; Hosseini, M.; Ganjali, M. R. Visual Detection of MiRNA Using Peroxidase-like Catalytic Activity of DNA-CuNCs and Methylene Blue as Indicator. *Clin. Chim. Acta* **2018**, *483*, 119−125.
(158) Dehghani, Z.; Hosseini, M.; Mohammadnejad, J.; Ganjali, M. R. New Colorimetric DNA Sensor for Detection of Campylobacter Jejuni in Milk Sample Based on Peroxidase-Like Activity of Gold/Platinium Nanocluster. *ChemistrySelect* **2019**, *4* (40), 11687−11692.
(159) Teng, Y.; Shi, J.; Pong, P. W. T. Sensitive and Specific Colorimetric Detection of Cancer Cells Based on Folate-Conjugated Gold−Iron-Oxide Composite Nanoparticles. *ACS Appl. Nano Mater.* **2019**, *2* (11), 7421−7431.
(160) Mollasalehi, H.; Shajari, E. A Colorimetric Nano-Biosensor for Simultaneous Detection of Prevalent Cancers Using Unamplified Cell-Free Ribonucleic Acid Biomarkers. *Bioorg. Chem.* **2021**, *107*, No. 104605.
(161) Yu, T.; Dai, P. P.; Xu, J. J.; Chen, H. Y. Highly Sensitive Colorimetric Cancer Cell Detection Based on Dual Signal Amplification. *ACS Appl. Mater. Interfaces* **2016**, *8* (7), 4434−4441.
(162) Kim, S.; Kim, T. G.; Lee, S. H.; Kim, W.; Bang, A.; Moon, S. W.; Song, J.; Shin, J.-H.; Yu, J. S.; Choi, S. Label-Free Surface-Enhanced Raman Spectroscopy Biosensor for On-Site Breast Cancer Detection Using Human Tears. *ACS Appl. Mater. Interfaces* **2020**, *12* (7), 7897−7904.
(163) Zhang, L.; Mu, C.; Zhang, T.; Wang, Y.; Wang, Y.; Fan, L.; Liu, C.; Chen, H.; Shen, J.; Wei, K.; Li, H. Systemic Delivery of Aptamer-Conjugated XBP1 SiRNA Nanoparticles for Efficient Suppression of HER2+ Breast Cancer. *ACS Appl. Mater. Interfaces* **2020**, *12* (29), 32360−32371.
(164) Tao, Y.; Li, M.; Kim, B.; Auguste, D. T. Incorporating Gold Nanoclusters and Target-Directed Liposomes as a Synergistic Amplified Colorimetric Sensor for HER2-Positive Breast Cancer Cell Detection. *Theranostics* **2017**, *7*, 899−911.
(165) Li, M.; Lao, Y.-H.; Mintz, R. L.; Chen, Z.; Shao, D.; Hu, H.; Wang, H.-X.; Tao, Y.; Leong, K. W. A Multifunctional Mesoporous Silica-Gold Nanocluster Hybrid Platform for Selective Breast Cancer Cell Detection Using a Catalytic Amplification-Based Colorimetric Assay. *Nanoscale* **2019**, *11*, 2631−2636.
(166) Luo, D.; Wang, X.; Zeng, S.; Ramamurthy, G.; Burda, C.; Basilion, J. P. Targeted Gold Nanocluster-Enhanced Radiotherapy of Prostate Cancer. *Small* **2019**, *15* (34), 1900968.
(167) Yoo, S.; Gujrathi, I.; Haider, M. A.; Khalvati, F. Prostate Cancer Detection Using Deep Convolutional Neural Networks. *Sci. Rep.* **2019**, *9* (1), 1−10.
(168) Chan, K. M.; Gleadle, J.; O'Callaghan, M.; Vasilev, K.; Macgregor, M. Prostate Cancer Detection: A Systematic Review of Urinary Biosensors. *Prostate Cancer Prostatic Dis* **2022**, *25*, 39.
(169) Abarghoei, S.; Fakhri, N.; Borghei, Y. S.; Hosseini, M.; Ganjali, M. R. A Colorimetric Paper Sensor for Citrate as Biomarker for Early Stage Detection of Prostate Cancer Based on Peroxidase-like Activity of Cysteine-Capped Gold Nanoclusters. *Spectrochim. Acta - Part A Mol. Biomol. Spectrosc.* **2019**, *210*, 251−259.
(170) Shamsipur, M.; Naseri, M. T.; Babri, M. Quantification of Candidate Prostate Cancer Metabolite Biomarkers in Urine Using Dispersive Derivatization Liquid-Liquid Microextraction Followed by Gas and Liquid Chromatography-Mass Spectrometry. *J. Pharm. Biomed. Anal.* **2013**, *81−82*, 65−75.

https://doi.org/10.1021/acsomega.3c06884
ACS Omega 2024, 9, 3143−3163